

A biogeochemical modeling study on microbiological response to high CO₂

Qusheng Jin*, Department of Geological Sciences, University of Oregon, Eugene, OR, USA.
Matthew F. Kirk, Department of Geology, Kansas State University, Manhattan, KS, USA.

Correspondence:

Qusheng Jin
qjin@uoregon.edu

Running title: Thermodynamics and kinetics of microbial reactions under high CO₂

Abstract

Geological carbon sequestration captures CO₂ from industrial sources and stores the captured CO₂ in subsurface reservoirs, a viable strategy for mitigating global climate change. In assessing the environmental impact of the strategy, a key question is how biogeochemical processes may respond to the elevated CO₂ concentration. This study took a biogeochemical modeling approach and investigated the influence of high CO₂ partial pressures on the thermodynamics and kinetics of microbial reactions. The simulation considered common microbial reactions in subsurface environments, including syntrophic oxidation, iron reduction, sulfate reduction, and methanogenesis. The modeling results showed that increasing CO₂ partial pressures decreases groundwater pH and impacts chemical speciation of dissolved inorganic carbon and weak acids, which in turn affect microbial reactions in different ways and to different extents. Specifically, the thermodynamic analysis showed that increasing CO₂ partial pressure lowers the energy available from syntrophic oxidation and acetoclastic methanogenesis, but raises the available energy of microbial iron reduction and hydrogenotrophic sulfate reduction and methanogenesis. The kinetic modeling suggested that high CO₂ partial pressure has the potential of inhibiting microbial sulfate reduction, while promoting microbial iron reduction. These results highlight the complexity in microbiological responses to elevated CO₂ abundance, and the potential power of biogeochemical modeling in evaluating and quantifying these responses.

Keywords: biogeochemical modeling, available energy, microbial kinetics, carbon sequestration, iron reduction, sulfate reduction

1. Introduction

Carbon capture and geological storage is one option in the range of actions that help stabilize atmospheric CO₂ levels despite anticipated increases in fossil fuel combustion (IPCC, 2005). Geological carbon sequestration involves capturing CO₂ before its emission into the atmosphere and injecting it into a deep subsurface reservoir (Benson and Cole, 2008). The technology injects CO₂ at depths >800 m, where CO₂ would exist as a buoyant supercritical phase (IPCC, 2005). A low-permeability caprock overlying a storage reservoir can provide structural trapping that limits upward migration of CO₂. Over time, CO₂ would also be trapped by dissolution into water, formation of minerals, and capillary trapping (Benson and Cole, 2008).

Although geological carbon sequestration is promising, it has the potential to negatively affect groundwater resources. CO₂ or CO₂-rich brine from deep storage reservoirs can diffuse through caprocks, and migrate upwards through faults and fractures, and abandoned wells (IPCC, 2005; Celia and Nordbotten, 2009; Keating et al., 2013; Keating et al., 2014). The leakage of CO₂ negatively affects the water quality of overlying freshwater aquifers, and has been described in detail previously (e.g., Kharaka et al., 2006; Lu et al., 2010; Wilkin and Digiulio, 2010; Harvey et al., 2013; Humez et al., 2014; Lions et al., 2014; Shao et al., 2015). Briefly, CO₂ leakage can lower groundwater pH, increase salinity, dissolve aquifer minerals, and mobilize hazardous solutes (Wang and Jaffe, 2004; Zheng et al., 2009; Apps et al., 2010; Kharaka et al., 2010; Little and Jackson, 2010; Lu et al., 2010; Wilkin and Digiulio, 2010). The CO₂ could also eventually reach the atmosphere, undermining the attempts to hold atmospheric CO₂ levels in check.

CO₂ leakage affects microorganisms living in aquifers. CO₂ of extremely high pressure can kill microbes by extracting intracellular materials, disabling enzymes, and mobilizing toxic trace elements from minerals (Bertoloni et al., 2006; Oule et al., 2006; Wimmer and Zarevucka, 2010; Santillan et al., 2013). Nevertheless, microorganisms are likely to persist in aquifers exposed to CO₂ leakage (Kirk et al., 2016). Numerous studies have observed microorganisms in environments with dissolved CO₂ levels that are high relative to those of most natural waters (Yakimov et al., 2002; Inagaki et al., 2006; Videmsek et al., 2009; Oppermann et al., 2010; Emerson et al., 2015). Recently, Peet et al. (2015) documented microbial growth in the presence of supercritical CO₂. Microbial tolerance to high-pressure CO₂ is enhanced for cells that possess Gram positive cell walls, grow within biofilms, and produce spores (Zhang et al., 2006; Mitchell et al., 2008). Microbial survival can also be promoted by aquifer minerals capable of rapid pH buffering (Wu et al., 2010).

Many questions still remain to be addressed in order to assess the impact of CO₂ leakage on subsurface microbiology (Harvey et al., 2013). For example, how does CO₂ leakage affect microbial energetics and the interactions between different microorganisms? Filling this knowledge gap is important because microorganisms can affect not only the chemical composition of aquifers but also the flow of groundwater (Gerlach and Cunningham, 2010; Flynn et al., 2013). Many microbial reactions consume protons, which enhances the dissolution of CO₂ gas. As a result, the impact of CO₂ leakage on aquifer microorganisms may also affect the fate of CO₂ migrating into aquifers.

In this study, we use biogeochemical modeling to investigate how CO₂ leakage may influence the thermodynamics and kinetics of microbial reactions in aquifers. Specifically, we first explore how CO₂ leakage impacts aquifer geochemical properties that are relevant to microbial reactions. We then simulate how CO₂ leakage affects the thermodynamics of syntrophic oxidation, iron reduction, sulfate reduction, and methanogenesis. We also carry out kinetic modeling to explore how CO₂ leakage influences the occurrence and activity of microorganisms in an aquifer. Our results show that CO₂ leakage significantly impacts the thermodynamics and kinetics of microbial reactions, and can change the outcome of microbial interactions.

2. Methods

2.1. Hypothetical aquifers

The simulation considers two hypothetical aquifers, a carbonate-free aquifer and a calcite-rich aquifer, that are subject to CO₂ leakage from deep storage reservoirs (fig 1). The carbonate-free aquifer has no carbonate mineral, and the calcite-rich aquifer contains abundant calcite as a representative carbonate mineral. In the aquifers, groundwater contains 10 mM Na⁺, 9 mM Cl⁻, 5 mM bicarbonate, and 2 mM Ca²⁺ flows through at a flow rate of 5 cm·yr⁻¹. Both the chemical composition and the flow rate are within the ranges reported for deep aquifers (Chapelle, 2001).

CO₂ leaks into the hypothetical aquifers from deep reservoirs via a fault. The simulation describes the progress of CO₂ leakage by raising CO₂ partial pressure of the groundwater. A wide range of CO₂ partial pressures are possible during CO₂ leakage. The simulation assumes a maximum value of 30 atm, which equates to one-third of total pressure typical for underground drinking water resources (Wilkin and Digiulio, 2010).

The inclusion of the carbonate-free and the calcite-rich aquifer is to account for the wide range in the responses of pH to CO₂ leakage. Specifically, CO₂ leakage into groundwater of circumneutral pH induces a hydrolysis reaction,



which decreases groundwater pH. The decrease in groundwater pH depends in part on mineral compositions of aquifers (e.g., Gunter et al., 1997; Xu et al., 2005; Kampman et al., 2009; Matter and Kelemen, 2009). For example, proton reacts with carbonate minerals, and these reactions buffer the change in pH. Taking calcite (CaCO₃) as an example, proton reacts rapidly with this mineral,



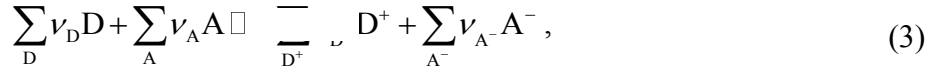
Proton also reacts with silicate minerals, such as feldspars and clay minerals, releasing aluminum and silicate into groundwater. These reactions are typically much slower than the dissolution of carbonate minerals (Sherlock et al., 1995; Gunter et al., 1997; Gislason et al., 2010; Wilkin and Digiulio, 2010). As a result, over relatively short time scales, these reactions are not as effective as the dissolution of carbonate minerals in pH buffering. Another proton-consuming reaction is the sorption onto the surface of clay minerals, metal oxides and hydroxides, and other minerals of large surface areas. Compared to mineral dissolution, the impact of surface complexation on groundwater pH is relatively insignificant.

2.2. Microbial reactions

Aquifers house diverse microorganisms, which can be separated into a series of functional groups, including fermenters, syntrophs, and respirers (Jin and Roden, 2011). Fermenting microbes degrade natural organic matter to H₂, acetate, lactate, propionate, and other short-chain fatty acids, and to methanol, ethanol, and other primary alcohols. Syntrophs oxidize short-chain fatty acids and primary alcohols to acetate and CO₂, and transfer the released electrons to the reduction of protons to dihydrogen (H₂). On the other hand, respirers oxidize H₂, short-chain fatty acids and primary alcohols, and transfer the released electrons to the reduction

of O₂, ferric minerals, sulfate, bicarbonate, and other electron acceptors.

The redox reactions catalyzed by syntrophs and respirers can be represented as



where D and D⁺ are electron donors and their oxidized forms, respectively, A and A⁻ are electron acceptors and their reduced forms, respectively, and ν_D and others are stoichiometric coefficients. In microbiology and biochemistry, the thermodynamics of redox reactions is commonly characterized using reduction potential. Specifically, for the redox couple of D and D⁺, the reduction potential E_D (V) is calculated according to

$$E_D = E_D^{\circ'} - \frac{RT}{nF} \cdot \left[\ln \left(\prod_D \gamma_D^{\nu_D} \cdot m_D^{\nu_D} \right) - \ln \left(\prod_{D^+} \gamma_{D^+}^{\nu_{D^+}} \cdot m_{D^+}^{\nu_{D^+}} \right) \right]; \quad (4)$$

for the redox couple of A and A⁻, the reduction potential E_A is calculated as

$$E_A = E_A^{\circ'} - \frac{RT}{nF} \cdot \left[\ln \left(\prod_{A^-} \gamma_{A^-} \cdot m_{A^-} \right) - \ln \left(\prod_A \gamma_A \cdot m_A \right) \right]. \quad (5)$$

Here $E_D^{\circ'}$ and $E_A^{\circ'}$ are standard potentials at pH 7, n is the number of electrons transferred per reaction, γ_D and others are activity coefficients (M⁻¹), m_D and others are molal concentrations, R is the gas constant (J·mol⁻¹·K⁻¹), F is the Faraday's constant, and T is the absolute temperature (K). Table 1 lists the reduction reactions of redox couples commonly found in aquifers and the standard reduction potentials ($E_D^{\circ'}$ and $E_A^{\circ'}$) at 1 atm, 25 °C, and pH 7. For the purpose of comparing stoichiometric coefficients of proton and bicarbonate, the reactions are written in terms of eight electron transfer ($n = 8$).

By transferring electrons, syntrophs and respirers liberate the chemical energy from redox reactions, which become available to their metabolisms. The available energy ΔG_A [J·(mol reaction)⁻¹, or J·mol⁻¹] is the negative of the Gibbs free energy change of redox reactions, and is calculated from

$$\Delta G_A = nF \cdot (E_A - E_D), \quad (6)$$

the difference in the reduction potentials between electron acceptors E_A and donors E_D . Table 2 lists the standard available energy at 1 atm, 25 °C, and pH 7 for common redox reactions in aquifers.

The rate r (M·s⁻¹) at which syntrophs and respirers catalyze redox reactions can be calculated according to the thermodynamically consistent rate law (Jin and Bethke, 2003;2005;2007):

$$r = k \cdot [X] \cdot F_D \cdot F_A \cdot F_T, \quad (7)$$

where k is the rate constant [mol·(g dry weight)⁻¹·s⁻¹, or mol·g⁻¹·s⁻¹], $[X]$ is the biomass concentration [g dry weight·(kg H₂O)⁻¹, or g·kg⁻¹], F_D and F_A are the kinetic factors of electron donor and acceptor, respectively, and F_T is the thermodynamic potential factor. The kinetic factors are calculated according to

$$F_D = \frac{m_D}{K_D + m_D}, \quad (8)$$

$$F_A = \frac{m_A}{K_A + m_A}, \quad (9)$$

where K_D and K_A are the half-saturation constants (M) for electron donor D and acceptor A, respectively. The thermodynamic factor is calculated according to

$$F_T = 1 - \exp\left(-\frac{\Delta G_A - \Delta G_C}{\chi \cdot RT}\right) \quad (10)$$

where ΔG_C (J·mol⁻¹) represents the energy saved by microbes, and χ is the average stoichiometric number. The saved energy ΔG_C is calculated as

$$\Delta G_C = m_p \cdot \Delta G_p \quad (11)$$

the product of the ATP yield m_p of microbial reaction, and the phosphorylation energy ΔG_p , i.e., the energy required to synthesize ATP from ADP and phosphate in the cytoplasm of microorganisms. In this study, the value of ΔG_p is taken as 45 kJ·(mol ATP)⁻¹ (Jin, 2012).

For microbial reduction of ferric minerals, its rate depends on the molal concentration $m_{\text{surf,avail}}$ of bioavailable surface sites of the minerals. According to Roden (2006);2008), the rate can be calculated according to

$$r = k_{\text{surf}} \cdot m_{\text{surf,avail}} \cdot \frac{[X] / m_{\text{surf,avail}}}{K_A^{\text{surf,avail}} + [X] / m_{\text{surf,avail}}} \cdot F_D \cdot F_T, \quad (12)$$

where k_{surf} is the bioavailable site-specific rate constant (s⁻¹), and $K_A^{\text{surf,avail}}$ is a constant in g cell dry weight per mol bioavailable surface sites (g·mol⁻¹). The concentrations $m_{\text{surf,avail}}$ of bioavailable surface sites are influenced by the sorption of ferrous iron on ferric minerals (Roden and Urrutia, 2002).

Syntrophs and respirers utilize the saved energy ΔG_C to synthesize biomass. The rate at which the biomass concentration $[X]$ changes with time is calculated

$$\frac{d[X]}{dt} = (\mu - D) \cdot [X], \quad (13)$$

where μ is the specific growth rate (s⁻¹), and D is the specific rate of maintenance (s⁻¹). The specific growth rate μ is calculated according to

$$\mu = Y \cdot \frac{r}{[X]}. \quad (14)$$

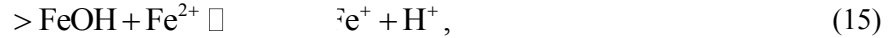
Here Y is the growth yield, the grams of biomass synthesized per mol reaction (g·mol⁻¹).

2.3. Model implementation

We carried out the simulation using the React program of the software package Geochemist's Workbench version 9.0 (Bethke, 2008). Following common practice in geochemical reaction modeling (Bethke, 2008), the simulation assumes that aqueous chemical speciation is at thermodynamic equilibrium, and describes these reactions on the basis of the

updated LLNL Thermodynamic Database (Delany and Lundeen, 1990). This database was modified to include amorphous iron sulfide (solubility product of $10^{-2.96}$) (Langmuir, 1997), and goethite (solubility product of $10^{1.40}$) (Bigham et al., 1996). The activity coefficients are calculated according to an extended form of the Debye-Hückel equation (Helgeson, 1969).

Aquifers may contain various ferric minerals. The simulation takes goethite as a representative, and describes the sorption of ferrous iron onto the surface of goethite using non-electrostatic Langmuir-style adsorption isotherms (Stumm and Morgan, 1996). Specifically, the sorption reaction is



where $>\text{FeOH}$ represents the native surface site that is available to bioreduction, and $>\text{FeOFe}^+$ is ferrous iron surface species. The logarithmic equilibrium constant of the reaction is -2.50 (Jin and Roden, 2011). The value of $m_{\text{surf,avail}}$ is calculated as the difference in concentration between the total surface sites and those occupied by sorbed ferrous iron.

3. Results and discussion

3.1. Groundwater chemistry

Figure 2, 3, and 4 shows, according to the simulation results, how groundwater chemistry responds to the increase in CO_2 partial pressure. Before CO_2 from the deep reservoir reaches the hypothetical aquifers, the groundwater has pH of 8 and a partial pressure of CO_2 of 3.1×10^{-4} atm. Dissolved inorganic carbon occurs mainly as bicarbonate (0.5 mM), dissolved CO_2 (0.01 mM), and calcium-bicarbonate complex species (CaHCO_3^+ , 0.01 mM).

3.1.1. pH and inorganic carbon

CO_2 leakage raises the CO_2 partial pressures to 30 atm. According to the simulation results (figs 2), the increase in CO_2 partial pressure lowers significantly groundwater pH, and raises the concentration of dissolved CO_2 in the aquifers. Specifically, in the carbonate-free aquifer, where CO_2 partial pressure increases from near 0 to 30 atm, pH decreases from 8 to 3.5, and dissolved CO_2 concentration increases to 1.06 M. But there is relatively little increase in the concentration of bicarbonate or calcium-bicarbonate complex (CaHCO_3^+).

In the calcite-rich aquifer, the increase in CO_2 partial pressure also raises the concentration of dissolved CO_2 to 1.06 M, but decreases groundwater pH only to 5. In addition, the increase in CO_2 partial pressure also increases significantly the concentrations of bicarbonate and CaHCO_3^+ ; bicarbonate and CaHCO_3^+ concentrations increase to 60.5 mM and 10.4 mM, respectively, at CO_2 partial pressure of 30 atm.

The different responses of the two aquifers arise from CO_2 -induced dissolution of calcite. In the carbonate-free aquifer, the simulation does not consider any reaction that consumes protons. As a result, most of the protons generated by CO_2 dissolution stay in the groundwater, lowering pH significantly. In comparison, in the calcite-rich aquifer, protons react with calcite, which buffers the decrease in pH, and adds bicarbonate to the groundwater.

The simulation results agree with previous assessment. The magnitude of pH decrease by CO₂ addition depends on the extent to which the environment can buffer CO₂ acidity as well as the pressure, temperature, and salinity of subsurface fluids. The solubility of CO₂ increases with pressure and thus depth but decreases with temperature and salinity (Benson and Cole, 2008). Decreases in the pH of fresh groundwater observed by field and laboratory studies range from 0.8 to 2.9 pH units (Lions et al., 2014). Similarly, geochemical modeling analysis indicates that, during CO₂ injection experiment in the Frio Formation, the pH of basin brine under subsurface conditions decreased from about 6.5 to 3 (Kharaka et al., 2009).

3.1.2. Aqueous speciation

The pH decrease in groundwater has a direct impact on the speciation of dissolved chemicals. Figure 3 shows how CO₂ leakage changes the relative abundances of acetate, lactate, propionate, butyrate, monohydrogen sulfide (HS⁻), and their conjugate acids. These chemical species directly participate in microbial redox reactions.

The response of aqueous speciation is more pronounced in the carbonate-free aquifer than in the calcite-rich aquifer. In the carbonate-free aquifer (fig 3A), the relative abundances of different acids increase, while the relative abundances of the conjugate bases decrease, with the increase in CO₂ partial pressure. The appearance of the cross-over points for the acids and their conjugate bases follows the sequence of the acidity constants. Among these acids, dihydrogen sulfide (H₂S) has the largest logarithmic acidity constant pK_a of 7.0 (Lide, 2003), and H₂S and HS⁻ reach equal concentrations where CO₂ partial pressure increases to 4×10⁻³ atm, and groundwater pH decreases to 7.0. On the other hand, lactic acid has the smallest pK_a of 3.86, and lactic acid and lactate take the same concentration where CO₂ partial pressure reaches 12 atm, and groundwater pH drops to 3.86.

In the calcite-rich aquifer (fig 3B), only the speciation of dihydrogen sulfide shows significant variations. Specifically, increases in CO₂ partial pressure converts monohydrogen sulfide to dihydrogen sulfide. At CO₂ partial pressure of 2.9×10⁻² atm and pH of 7, the two species have the same concentration. The speciations of acetic acid, propionic acid, and butyric acid also respond to the increase in CO₂ partial pressure, but to a much lesser extent. These acids occur at relatively significant concentrations, only after CO₂ partial pressure increase over 1 atm and pH decreases to 6. The modest responses of aqueous speciation in the calcite-rich aquifer arises from the limited decrease in groundwater pH (fig 2C).

3.1.3. Ionic strength and activity coefficient

In the calcite-rich aquifer, CO₂ leakage also raises the ionic strength of the groundwater (fig 4A). Where CO₂ partial pressure increases from 3.0×10⁻⁴ to 30 atm, the ionic strength increases from 16.6 mM to 100 mM. This increase is mainly due to the increases in the concentrations of Ca²⁺ and bicarbonate by the dissolution of calcite (fig 2D). In comparison, in the carbonate-free aquifer, the ionic strength of groundwater remains constant with the increase in CO₂ partial pressure (data not shown).

Ionic strength controls the thermodynamic properties of dissolved chemical species, which can be quantified using activity coefficient (eq 4 and 5, fig 4B). Among different theories, the extended Debye-Hückel equation, or the B-dot equation, represents a robust choice applicable for Na/Cl-dominated solution of ionic strength up to 2 molal (Helgeson, 1969). According to the B-dot equation, activity coefficients depend significantly on the ionic strength of groundwater and the charges of chemical species. Figure 4B shows in the calcite-rich aquifer, the activity coefficients of ions decrease with the increases in CO₂ partial pressure, because of the increase in the ionic strength. For chemical species with +1 or -1 charge, where CO₂ partial pressure increases from near 0 to 30 atm, the activity coefficients decrease by about 0.1, from near 0.89 to 0.77. For those with +2 or -2 charge, the activity coefficients decrease by about 0.2, from near 0.6 to 0.4. For neutral chemical species, the activity coefficients are set at unity, and do not change with the ionic strength of groundwater.

3.2. Reduction potential

The above geochemical variations place a fundamental constraint on the thermodynamics of microbial reactions. This thermodynamic impact can be evaluated using the reduction potentials of redox couples in microbial reactions. Here we focus on the electron donors produced by the degradation of natural organic matter, include dihydrogen (H₂), acetate, lactate, propionate, butyrate, methanol, and ethanol, and consider the common electron acceptors in aquifers, such as goethite, sulfate, bicarbonate, and proton (Lovley and Chapelle, 1995; Bethke et al., 2011).

We compute the change in reduction potential, not absolute value, for each electron donor and acceptor. In this way, we highlight the significance by which CO₂ leakage affects the reduction potentials. Using the change, not absolute value, also avoids the need of the concentrations of electron donors and acceptors. In aquifers, there are few concentration measurements for lactate, propionate, butyrate, methanol, and ethanol. On the other hand, for the electron acceptors of sulfate and bicarbonate, their concentrations vary over orders of magnitude (Kirk et al., 2015). Using the changes also simplifies the discussion of ferric mineral reduction. In aquifers, different ferric minerals, such as ferrihydrite, goethite, hematite, and lepidocrocite, may be present. Although these ferric minerals have different reduction potentials, their reduction potentials respond in the same fashion to pH variations, because the reduction of these ferric minerals consumes the same number of protons per electron. Here we evaluate the changes in the reduction potential of goethite, but the result is applicable to ferrihydrite, hematite, and lepidocrocite.

Figure 5 shows, according to the simulation results, how reduction potentials of different redox couples respond to the leakage of CO₂. In both the carbonate-free and calcite-rich aquifers, the reduction potentials increase with CO₂ partial pressures. For the redox couples considered by this study (see table 1), their reduction reactions consume protons and, as a result, their reduction potentials increase with the decrease in groundwater pH (eqs 4 and 5).

3.2.1. Carbonate-free aquifer

In the carbonate-free aquifer, the significances of the changes in reduction potentials

depend primarily on groundwater pH and the stoichiometric coefficients of protons in the reduction reactions of redox couples. Reduction reactions of different redox couples have different stoichiometric coefficients of protons (table 1). For example, the reduction of H^+ to H_2 consumes eight protons per eight electrons, while the reduction of Fe^{2+} to goethite consumes 24 protons per eight electrons. As a result, the increase in the reduction potential of the redox couple of H^+/H_2 is the smallest, 267.8 mV, while the increase for the couple of Fe^{2+} /goethite is the largest, 639.5 mV. The reduction reaction of other redox couples consumes 9 to 10 protons per eight electrons, close to the stoichiometric coefficient of protons in the redox couple of H^+/H_2 . As a result, the changes in the reduction potentials of these redox couples are larger than, but close to, the change in the potential of H^+ reduction to H_2 .

3.2.2. Calcite-rich aquifer

Compared to those in the carbonate-free aquifer, the increases in reduction potentials are relatively small in the calcite-rich aquifer. These small increases arise from the limited decrease in pH induced by CO_2 leakage. Specifically, where CO_2 partial pressure increases from near 0 to 30 atm, groundwater pH decreases only by 3 units (fig 2C). As a result, the reduction potential of H^+/H_2 increases by 176.1 mV, and that of Fe^{2+} /goethite increases by 391.2 mV.

For the redox couples of acetate, lactate, propionate, and methanol, their reduction reactions consume bicarbonate (table 1). As a result, their reduction potentials also vary with bicarbonate concentration or activity. Specifically, the reduction potentials depend on the stoichiometric coefficients of bicarbonate anion in reduction reactions of the redox couples, and the changes in the concentration of bicarbonate. Where CO_2 partial pressure increases from near 0 to 30 atm, the activity of bicarbonate increases by about one order of magnitude because of the increase in concentration (fig 2D). The stoichiometric coefficient of bicarbonate varies from 1 per eight electrons in the reduction reaction of methane to 2 per eight electrons in the reduction reactions of acetate and lactate. As a result, the increases in the reduction potentials of acetate and lactate with CO_2 partial pressure are faster than that of HCO_3^- /methane (fig 5B).

3.3. Available energy

The above calculation of reduction potentials illustrates the impact of CO_2 leakage on individual electron donors and acceptors. But the results are not straightforward in illustrating the thermodynamic response of microbial reactions. This is because, for the common redox couples in aquifers (table 1), their reduction potentials all respond positively with the increase in CO_2 partial pressure (fig 5). A direct thermodynamic assessment of microbial reactions is the energy available to microbial functional groups. The available energy is a key geochemical parameter that controls both the rates of microbial reactions and the growth of functional groups (Jin, 2012).

We compute the energy available from microbial reactions that transfer eight electrons (table 2). The only exception is the energy available from acetoclastic methanogenesis, which is computed in terms of one acetate. We compute the energy available to the common functional groups in aquifers, including syntrophs, ferric iron reducers, sulfate reducers, and methanogens (table 2). For the same reasons in evaluating reduction potentials, we focus on the changes in the

available energy, not the absolute values. Figure 6 shows how the energy available to the microbial functional groups responds to the leakage of CO₂.

3.3.1. Syntroph

The simulation results show that CO₂ leakage decreases the energy available to syntrophs (fig 6A and E). The energy available to syntrophs depends on groundwater pH, because protons are produced by the syntrophic oxidation of short-chain fatty acids and alcohols (table 2). In both the carbonate-free and calcite-rich aquifers, CO₂ leakage decreases groundwater pH (fig 2A and C), thereby lowering the energy available to syntrophs.

The energy available to syntrophs may also depend on bicarbonate concentrations (table 2). Specifically, the oxidation of acetate, lactate, propionate, and methanol produces bicarbonate ions. As a result, the energy released by these reactions depends on the concentrations of bicarbonate; increase in bicarbonate concentration decreases the available energy. In the calcite-rich aquifer, the decrease in pH is less than that in the carbonate-free aquifer, but the increase in bicarbonate concentration is more significant than in the carbonate-free aquifer. Overall, the effect of increasing bicarbonate concentrations takes its toll, leading to greater decreases in available energies in the calcite-rich aquifer than in the carbonate-free aquifer.

In comparison, the syntrophic oxidation of butyrate and ethanol does not generate bicarbonate, and thus the available energy depends primarily on groundwater pH. Because the pH decrease is more significant in the carbonate-free aquifer than in the calcite-rich aquifer, the available energy to butyrate- and ethanol-oxidizing syntrophs decrease more significantly in the carbonate-free aquifer than in the calcite-rich aquifer.

It is interesting to note that in the carbonate-free aquifer, for both butyrate- and ethanol-oxidizing syntrophs, the variations in the available energy level off at CO₂ partial pressures greater than 1 atm. This is because the increase in CO₂ partial pressure decreases groundwater pH, which in turn decreases the concentration of acetate (fig 3). At CO₂ partial pressures above 1 atm, pH decreases below 5, and acetate concentration is less than half of the total concentration of acetate and acetic acid (fig 3A). Acetate is one of the products of the syntrophic oxidation of butyrate and ethanol. For this reason, the decrease in acetate concentration increases the energy available to butyrate- and ethanol-oxidizing syntrophs, which counteracts the decreases in the available energy by the pH decrease.

In comparison, in the carbonate-rich aquifer, the available energy of butyrate- and ethanol-oxidizing syntrophs decreases steadily with the increase in CO₂ partial pressure. This is because of the modest pH decrease in this aquifer. At CO₂ partial pressure of 1 atm, groundwater pH is about 6, and compared to acetic acid, acetate still remains as the dominant form (fig 3B).

3.3.2. Iron reducer

The simulation results show that CO₂ leakage raises the energy available to iron reducers that utilize different electron donors (see table 2, fig 6B and F). Like in the above case of syntrophic oxidation, pH is also a key parameter in determining the available energy. But in the

reduction of goethite coupled to the oxidation of different electron donors, protons are the reactants and, as a result, the available energy increases with the decrease in pH. Also because the pH decrease is larger in the carbonate-free aquifer than in the calcite-rich aquifer, the increase in the available energy is more significant in the carbonate-free aquifer than in the calcite-rich aquifer.

In both aquifers, the increase in the available energy varies among different electron donors. Specifically, the decrease is most significant for H_2 oxidation, and least significant for lactate oxidation to acetate. This difference arises from the different stoichiometric coefficients of protons in goethite reduction coupled to the oxidation of different electron donors. The stoichiometric coefficient of protons in H_2 oxidation is the largest, while that in lactate oxidation to acetate is the smallest (table 2).

3.3.3. Sulfate reducer

For sulfate reducers, the responses of the energy available to CO_2 leakage are mixed. In the calcite-free aquifer (fig 6C), only the available energy of H_2 -oxidizing sulfate reducer increases significantly in response to CO_2 leakage. Where CO_2 partial pressure increases from near 0 to 30 atm, the available energy increases by $43.8 \text{ kJ}\cdot\text{mol}^{-1}$.

For sulfate reducers that oxidize other electron donors, their available energy responds to CO_2 leakage, but only marginally. Specifically, for sulfate reducers that oxidize acetate, propionate, and methanol, their available energy increases with CO_2 partial pressure, but only to a very small extent, less than $7.0 \text{ kJ}\cdot\text{mol}^{-1}$. For sulfate reducers that oxidize lactate, butyrate, and ethanol, their available energy first decreases with CO_2 leakage and then increase. Again, the variations remain less than $7.0 \text{ kJ}\cdot\text{mol}^{-1}$ over the increase in CO_2 partial pressure from near 0 to 30 atm.

Sulfate reduction by the oxidation of H_2 , acetate, propionate, and methanol consumes protons (table 2). As a result, the available energy increases with the increase in CO_2 partial pressure and the decrease in pH. The significance of the increases depends on the stoichiometric coefficients of protons in the reactions of sulfate reduction. Hydrogenotrophic sulfate reduction consumes most protons, and hence its available energy increases most significantly with the increase in CO_2 partial pressure.

In comparison, in sulfate reduction by the oxidation of acetate, propionate, and methanol, the stoichiometric coefficients of protons are relatively small, and the increases in the available energy by the pH decrease is also small. In addition, for acetate-oxidizing sulfate reduction, the increase in the available energy is also limited by the speciation of acetate and acetic acid. As shown in figure 3A, at CO_2 partial pressure above 1 atm, increase in the partial pressure decreases significantly acetate concentration, thereby decreasing the available energy.

For sulfate reduction that oxidizes lactate, butyrate, and ethanol, the initial decrease in the available energy can be explained by the production of protons under circumneutral pH condition. In writing the reaction equations for sulfate reduction, we assume that dihydrogen sulfide (H_2S) is the main species of dissolved sulfide. Under this assumption, no proton is

consumed by these reactions (table 2). But under circumneutral pH condition, a significant fraction of dissolved sulfide also occurs as monohydrogen sulfide (HS^-) (fig 3). If we replaced H_2S with HS^- in the reaction equations, sulfate reduction by the oxidation of lactate, butyrate, and ethanol would generate protons. This explains the slight decreases in the available energy at the beginning of CO_2 leakage, where pH of the groundwater is close to 7.

At CO_2 partial pressure above 0.1 atm, CO_2 leakage starts to turn groundwater from circumneutral to slightly acidic ($\text{pH} < 6$). Under this condition, H_2S becomes the only dominant sulfide species, no proton is produced by sulfate reduction, and the available energy is no longer dependent on pH.

At pH below 6, because of the pH control on aqueous speciation (fig 3A), the decrease in pH also starts to significantly lower acetate concentration. This explains the slight increase in the available energy by CO_2 partial pressure. Note that the speciation effect is relatively small for sulfate reduction by lactate oxidation. This is because lactate oxidation produces acetate, and the concentrations of both acetate and lactate decreases with the increase in CO_2 partial pressure.

In the calcite-rich aquifer (fig 6G), the energy available to hydrogenotrophic sulfate reducers increases during CO_2 leakage. For sulfate reducers using other electron donors, their available energy consistently decreases with the progress of CO_2 leakage. In this aquifer, the variations in the energy available to sulfate reducers results from the significant changes in both bicarbonate concentration and pH (fig 2C and D). Specifically, as discussed for the carbonate-free aquifer, under circumneutral pH condition, sulfate reduction by the oxidation of short-chain fatty acids and primary alcohols generates protons, and thus the available energy decreases with the increase in CO_2 partial pressure. For sulfate reduction that oxidizes acetate, lactate, propionate, and methanol, the available energy is further decreased by the significant increase in bicarbonate concentrations.

3.3.4. Methanogen

The simulation results show that in both the carbonate-free and calcite-rich aquifers, the available energy to hydrogenotrophic methanogenesis increases with the progress of CO_2 leakage, while that to acetoclastic methanogenesis decreases with the progress (fig 6D and H). The difference between the responses of the two pathways arises from the dependence of the available energy on both pH and the concentrations of acetate and bicarbonate in the groundwater. For hydrogenotrophic methanogenesis, it utilizes protons and bicarbonate as substrates, and hence its available energy increases with the decrease in pH and the increase in bicarbonate concentration. For acetoclastic methanogenesis, its available energy depends on the concentrations of acetate and bicarbonate. In the calcite-rich aquifer, CO_2 leakage raises significantly bicarbonate concentrations, thereby decreasing the energy available to acetoclastic methanogens. On the other hand, in the carbonate-free aquifer, the significant decrease in pH by CO_2 leakage converts acetate to acetic acid (fig 3A), which also decreases the available energy.

3.4. Microbial kinetics

The energy available from redox reactions controls the kinetics of microbial functional

groups (Jin and Bethke, 2007). According to the thermodynamically consistent rate law (eqs 7, 10, 13, and 14), increases in the available energy increase nonlinearly the rate of microbial respiration and hence the rate of microbial growth. On the other hand, decreases in the available energy decrease the rates of microbial respiration and growth. Based on the thermodynamic calculations (fig 6), CO₂ leakage may inhibit the metabolisms of syntrophs and acetoclastic methanogens, but promote the metabolisms of iron reducers and hydrogenotrophic sulfate reducers and methanogens. To demonstrate these impacts, we take as an example the hypothetical calcite-rich aquifer, and apply kinetic modeling to explore how the metabolisms of different microbial functional groups respond to the leakage of CO₂.

For illustration purpose, the simulation assumes that in the aquitard, microbial degradation of natural organic matter produce H₂, acetate, and lactate as the main products (fig 1). The simulation also assumes that these electron donors are produced at the same rate of $3.0 \times 10^{-7} \text{ mol} \cdot \text{liter}^{-1} \cdot \text{yr}^{-1}$. There are very few measurements of production rates of different electron donors in the subsurface, and the equal production rates in the simulation are purely assumptive. Nevertheless, the assumed rates are within the ranges reported for subsurface environments (Chapelle, 2001; Park et al., 2006), and are large enough to support different functional groups in the aquifer.

The simulation considers the functional groups of syntrophs, iron reducers, sulfate reducers, and methanogens that oxidize lactate to acetate, acetate to bicarbonate, and H₂ to protons. The redox reactions catalyzed by these functional groups form a reaction network that converts the degradation products of natural organic matter to bicarbonate and methane (fig 7). Simulating microbial metabolism requires a series of microbial kinetic, growth, and thermodynamic parameters (Jin and Roden, 2011; Jin et al., 2013). We assign the parameter values on the basis of previous studies, and the results are listed in table 3. The simulation seeded the functional groups with an initial biomass concentration of $10^{-9} \text{ g} \cdot \text{liter}^{-1}$.

Microbial kinetics depends on pH, temperature, and pressure of the environment (Ingraham, 1987), but how metabolic rates of different functional groups are controlled by these environmental factors still remains to be elucidated. Here we hold microbial kinetic and growth parameters constant to test whether the thermodynamic response to CO₂ leakage alone could provide a mechanism for changing the rates of microbial reactions. The simulation also assumes that the half-saturation constants describe the efficiency of microbes in utilizing the total dissolved electron donors or acceptors, not any specific chemical species. In other words, in computing kinetic factors (eqs 8 and 9), we only account for the total dissolved electron donors and acceptors, or the sum of the concentrations of acids and their conjugate forms.

There are two phases in the simulation (fig 8). During the first 400 years, there is no CO₂ leakage, but only the flow of the groundwater through the aquifer. As a result, the metabolisms of microbial functional groups depend on the chemical properties of the aquifer and the production of electron donors. In the second phase between 400 and 800 years, CO₂ from the deep reservoir arrives and, as a result, the partial pressure of CO₂ in the aquifer is assumed to increase linearly from $1.8 \times 10^{-3} \text{ atm}$ at year 400 to 30 atm at year 800.

As shown above (figs 2 to 4), CO₂ leakage significantly changes the chemistry of

groundwater. Specifically, at the time of year 400, where the leaked CO₂ first reaches the aquifer, groundwater pH decreases immediately from 8 to about 6 (fig 8B). Afterwards, pH decreases gradually to 5 over the next 400 years. The sharp decrease in pH is due to (1) the assumption that CO₂ partial pressure increases linearly with time to 30 atm over a period of 400 years, and (2) the fact that a pH drop from 8 to 6 only requires the production of about 1 μM proton in groundwater. In the hypothetical calcite-rich aquifer, a relatively small increase in CO₂ partial pressure from near 0 to 1 atm is sufficient to generate 1 μM proton (fig 2C). The subsequent gradual pH decrease can be explained by relatively large change in proton concentrations. An decrease in pH from 6 to 5 requires the production of about 10 μM protons, which can be generated by raising the partial pressure from 1 to 30 atm and by the simultaneous dissolution of CO₂ gas and calcite mineral into the groundwater. The simultaneous dissolution of CO₂ and calcite also increases bicarbonate concentration of groundwater (fig 2D).

3.4.1. Sulfate reduction

The thermodynamic analysis of microbial reactions suggests that CO₂ leakage has the potential of promoting hydrogenotrophic sulfate reduction, but inhibits sulfate reducers that oxidize acetate and lactate. To test this prediction, we assume that the groundwater contains 100 μM sulfate and 10 μM sulfide, and simulate the metabolisms of three different sulfate reducers that oxidize H₂, acetate, and lactate in the hypothetical calcite-rich aquifer.

According to the simulation results (fig 9), during the first simulation phase of 0 to 400 years, before CO₂ leakage takes place, all of the three sulfate reducers survive in the aquifer, and their metabolisms reach steady state. At steady state, microbial metabolisms produce 10.4 μM sulfide, 0.25 μM lactate, 0.05 μM acetate, and 20.3 nM H₂ in groundwater. The H₂-, acetate-, and lactate-oxidizing sulfate reducers reach a biomass concentration of 0.6, 1.8, and 0.5 μg·L⁻¹, respectively. The rates of sulfate reduction by oxidizing H₂, acetate, and lactate are 1.1×10^{-15} , 4.7×10^{-15} , and 4.1×10^{-16} M·s⁻¹, respectively. Thus, under the assumptions applied in the simulation, the aquifer is dominated by acetotrophic sulfate reduction, which accounts for 76% of total sulfate reduction.

The simulation results show that during the second phase of 400 to 800 years, the CO₂ leakage inhibits the metabolism of acetotrophic sulfate reducer, which agrees with the prediction of microbial thermodynamics. Specifically, both the biomass concentration and sulfate reduction rate decrease sharply – by 22% – during the first 90 years of CO₂ leakage. Afterwards, the biomass concentration and rate decrease almost linearly with time, and decrease to 1.1 μg·L⁻¹ and 2.9×10^{-15} M·s⁻¹, respectively, at year 800. Corresponding to the rate decrease, acetate concentration first increase to 0.12 μM at year 90, and then gradually increase to 0.17 μM at year 400.

The inhibition comes from the decrease in the available energy by CO₂ leakage, and can be evaluated using the thermodynamic factor F_T . This factor quantifies how the available energy, relative to the saved energy, controls microbial rate. As shown in figure 9E, before the CO₂ leakage, the energy available to acetotrophic sulfate reducer is 40.1 kJ·mol⁻¹, slightly larger than the saved energy, which is 33.75 kJ·mol⁻¹ (eq 11 and table 3). As a result, the thermodynamic factor takes a value of 0.35 (fig 9F). In the second phase, where CO₂ leakage takes place, the

available energy drops by $3.8 \text{ kJ}\cdot\text{mol}^{-1}$ during the first 90 years, and then decreases gradually to $35.5 \text{ kJ}\cdot\text{mol}^{-1}$ at year 800. The decrease in the available energy pulls down the thermodynamic factor to 0.11 at year 800.

The simulation also predicts that the CO_2 leakage ultimately drives acetotrophic sulfate reducers out of the aquifer. As shown in figure 9G, in addition to the thermodynamic factor, acetotrophic sulfate reduction is also limited by acetate and sulfate. The kinetic factors F_D and F_A quantify the extent by which acetate and sulfate limit the rate of sulfate reduction. Before the CO_2 leakage, because of small acetate concentration, the kinetic factor F_D of acetate is also small, only about 0.01. The kinetic factor of sulfate is relatively large, 0.72. Substituting these values, together with the thermodynamic factor F_T and the rate constant (see table 3) to the rate law (eq 7), acetotrophic sulfate reducer takes a specific growth rate of $1.0 \times 10^{-8} \text{ s}^{-1}$, which equates the assumed rate of specific maintenance, and hence allows the growth to reach a steady state.

But after the CO_2 leakage starts, the specific growth rate decreases because of the decrease in the available energy and the rate of acetotrophic sulfate reduction. Although the deceleration of acetotrophic sulfate reduction raises the concentration and hence the kinetic factor of acetate, the increase is not sufficient to offset the decrease by the decreasing available energy. As a result, the specific growth rate decreases below the specific maintenance rate, and the population size starts to decline and ultimately disappears from the aquifer.

The simulation results also show that during the second phase of 400 to 800 years, the CO_2 leakage has little influence on the metabolism of H_2 - or lactate-oxidizing sulfate reducers. According to the simulation results (fig 9C and D), both the biomass concentration and sulfate reduction rate of lactate-oxidizing sulfate reducer remain constant during CO_2 leakage. The biomass concentration and sulfate reduction rate of H_2 -oxidizing sulfate reducer increase, but only slightly – less than 6%.

In the case of sulfate reduction by lactate oxidation, the lack of response is due to the fact that in the hypothetical aquifer, this microbial reaction is not limited by the thermodynamic control. As shown in figure 9G, before the leakage of CO_2 , the available energy from lactate oxidation and sulfate reduction is $218.0 \text{ kJ}\cdot\text{mol}^{-1}$. After the CO_2 leakage, the available energy drops to $190.0 \text{ kJ}\cdot\text{mol}^{-1}$. These values are much larger than the energy saved by the lactate-oxidizing sulfate reducers, which is $101.25 \text{ kJ}\cdot\text{mol}^{-1}$ (see eq 11 and table 3). As a result, the thermodynamic factor F_T stays close to unity before and after the CO_2 leakage. In other words, although CO_2 leakage decreases the available energy, the decrease is not large enough to have any impact on microbial rates.

In the case of hydrogenotrophic sulfate reduction, the lack of response arises from the opposing effects of the increasing available energy and the decreasing H_2 concentration in groundwater. As shown in figure 9E and F, before CO_2 leakage, the energy available to hydrogenotrophic sulfate reducer is $47.4 \text{ kJ}\cdot\text{mol}^{-1}$, very close to the saved energy, which is $45 \text{ kJ}\cdot\text{mol}^{-1}$ (eq 11 and table 3). The thermodynamic factor F_T takes a value of 0.02. H_2 concentration is 21 nM, smaller than the assumed half-saturation constant of $1.1 \text{ }\mu\text{M}$ (table 3). The kinetic factor F_D takes a value of 0.02.

After the CO₂ leakage starts, the available energy increases, raising the thermodynamic factor F_T . At year 800, the available energy increases to 58.3 kJ·mol⁻¹, and the thermodynamic factor increases to 0.59, which increases the rate of H₂ oxidation. On the other hand, the increase in the rate of H₂ oxidation decreases the concentration of H₂, decreasing the kinetic factor F_D . At year 800, H₂ concentration decreases to 5.2 nM, and the kinetic factor F_D decreases to 0.005. According to the rate law (eq 7), the product of the thermodynamic and kinetic factors determines the rate of hydrogenotrophic sulfate reduction. Because the rate increase by increasing available energy balances the rate decrease by decreasing H₂ concentration, sulfate reduction rate does not change significantly by the leakage of CO₂.

3.4.2. Microbial competition

Microbial kinetics is a key to understanding the interactions among microbial functional groups. The above thermodynamic analysis suggests that CO₂ leakage promotes microbial iron reduction, but inhibits sulfate reducers that utilize short-chain fatty acids. As a result, CO₂ leakage may change the outcome of the competition between iron reducers and sulfate reducers.

To test this prediction, we simulate the metabolisms of iron reducers and sulfate reducers that oxidize H₂, acetate, and lactate in the hypothetical calcite-rich aquifer. We assume that the aquifer contains 1% goethite, and that the groundwater contains 1.0 mM sulfate, 10 μM sulfide, and 10 μM Fe²⁺. The assumed sulfate concentration is much larger than the half-saturation constants of sulfate reducers (table 3), which alleviates the limitation of sulfate on sulfate reduction rate. To consider other potential microbial interactions, the simulation also includes the metabolisms of lactate-oxidizing syntroph and hydrogenotrophic and acetoclastic methanogens. In this way, a total of nine functional groups are considered in the simulation.

Figure 10 show the results of the simulation. In the first 400 years, before CO₂ leakage takes place, out of the nine functional groups, only three survive in the aquifer, including lactate-oxidizing iron reducer, and hydrogenotrophic and acetotrophic sulfate reducers. In other words, under the assumptions applied in the simulation, lactate-oxidizing iron reducer competes successfully against its counterpart of sulfate reducers, but for both hydrogenotrophic and acetotrophic iron reducers, they are driven out of the aquifer by their counterparts of sulfate reducers. As a result, the production of H₂, acetate, and lactate in the aquitard supports simultaneously iron reduction and sulfate reduction in the aquifer.

After the metabolisms of the three groups reach steady state, the groundwater contains 5.8 μM Fe²⁺, 5.0 μM sulfide, 0.16 μM lactate, 25.2 nM acetate, and 11.4 nM H₂ in groundwater (fig 10A and B). In addition, there are two species on the surface of goethite, free or bioavailable surface sites (>FeOH) and sorbed ferrous iron (>FeOFe⁺), and their bulk concentrations are about 2 mM (fig 10C). At the steady state, the lactate-oxidizing iron reducer has a biomass concentration of 1.6 μg·L⁻¹, and the biomass concentrations of hydrogenotrophic and acetotrophic sulfate reducers are 0.57 and 2.45 μg·L⁻¹, respectively (fig 10D). The rate of iron reduction by lactate oxidation is 1.1×10⁻¹⁵ M·s⁻¹; the rates of hydrogenotrophic and acetotrophic sulfate reduction are 1.1×10⁻¹⁵ and 6.5×10⁻¹⁵ M·s⁻¹, respectively (fig 10E).

Between year 400 and 800, CO₂ leakage promotes the metabolism of acetotrophic and hydrogenotrophic iron reducers, and excludes acetotrophic and hydrogenotrophic sulfate reducer from the aquifer. At steady state, the aquifer contains acetotrophic and hydrogenotrophic iron reducers at 5.1 and 1.2 µg·L⁻¹, respectively. Acetotrophic and hydrogenotrophic iron reduction proceeds at a rate of 6.8×10^{-15} and 1.2×10^{-15} mol·L⁻¹·s⁻¹, respectively (fig 10D and E).

The CO₂ leakage promotes acetotrophic and hydrogenotrophic iron reduction by raising the energy available from the reduction of goethite. As shown in figure 10F, the CO₂ leakage increases significantly the energy available from goethite reduction coupled to the oxidation of acetate and H₂. At year 400, the available energy is only 64.0 kJ·mol⁻¹ for acetotrophic iron reduction, and 66.7 kJ·mol⁻¹ for hydrogenotrophic iron reduction. Both values are smaller than the energy saved by the two iron reducers; acetotrophic and hydrogenotrophic iron reducers save 67.5 and 90.0 kJ·mol⁻¹ of energy, respectively. Within 90 years, because of the sharp decrease in pH, the available energy of acetotrophic iron reduction increases to 260.0 kJ·mol⁻¹, and that of hydrogenotrophic iron reduction increases to 283.0 kJ·mol⁻¹. As a result, the thermodynamic factors of the two iron reducers increase from 0 at year 400 to near unity at year 490, and stay close to unity afterwards.

The CO₂ leakage also promotes microbial iron reduction by decreasing the concentration of sorbed ferrous iron and increasing the concentrations of bioavailable surface sites (fig 10C and eq 12). According to the rate law (eq 12), the rate of microbial iron reduction depends on the concentration of bioavailable surface sites of ferric minerals, which in turn depends on the sorption of ferrous iron. Ferrous iron sorption is controlled by pH; more ferrous iron sorbs onto the surface sites of goethite at large pH, and vice versa (Dixit and Hering, 2006). As shown in figure 10C, the decrease in pH by CO₂ leakage removes the sorbed ferrous iron from the surface sites of goethite, and thus makes available nearly all surface sites of goethite to iron reducers.

The increases in the available energy and the concentration of bioavailable surface sites raise the rates of iron reduction, which enable both hydrogenotrophic and acetotrophic iron reducers to compete successfully against sulfate reducers. Specifically, acetate and H₂ oxidation by the iron reducers decrease acetate and H₂ concentrations below 10 and 1 nM, respectively (fig 10A). The small acetate and H₂ concentrations decreases the specific growth rates of sulfate reducers below the specific maintenance rates, which leads to the death of the sulfate reducers.

Lactate-oxidizing syntroph and hydrogenotrophic and acetoclastic methanogens do not survive in the hypothetical aquifer, either before or after the leakage of CO₂. The absence of these functional groups is accounted for by the limited availability of electron donors, and by the relatively small yields *Y* of biomass synthesis. For example, at steady state, because of the small lactate concentration, the kinetic factor F_D of lactate for the syntroph is very small, only 3.2×10^{-6} . Neglecting the thermodynamic control, and substituting the kinetic factor and the growth yield to the rate law (eqs 7 and 13), the syntroph has a specific growth rate of 4.4×10^{-10} s⁻¹, much smaller than the specific maintenance rate of 10^{-8} s⁻¹ (table 3).

3.5. Implications for CO₂ trapping

CO₂ gas is buoyant and thus has the potential to migrate to the surface and escape to the

atmosphere. However, many microbial reactions consume protons, and thus have the potential of trapping CO₂ (table 2). By consuming protons, these reactions drive CO₂ hydrolysis reaction (eq 1) forward, converting CO₂ into bicarbonate and trapping CO₂ in the subsurface. By converting CO₂ into bicarbonate, carbon can be more securely stored within the aqueous phase and potentially precipitate as a carbonate mineral such as calcite, magnesite (MgCO₃), and siderite (FeCO₃). Mineral trapping is considered to be the most secure form of subsurface carbon trapping (Gunter et al., 1997).

The predicted changes in microbial activity by CO₂ leakage are favorable for CO₂ trapping. Because iron reduction consumes many more protons than sulfate reduction or methanogenesis (table 2), it has a much greater potential to generate bicarbonate. Per mole of acetate consumed, for example, iron reduction can generate 17 moles of bicarbonate whereas sulfate reduction only generates 3 moles of bicarbonate. As CO₂ is added into aquifers, a shift toward iron reduction would increase conversion of CO₂ into bicarbonate. Thus, an increase in the rate of iron reduction relative to the other reactions would act as a positive feedback mechanism on CO₂ trapping (Kirk et al., 2013).

Although it is well established that microbial reactions help neutralize acid mine water (e.g., Tuttle et al., 1969; Dean et al., 2013; Lindsay et al., 2015), the possibility that they could provide the same ecosystem service in geological carbon storage settings has received relatively little attention. The question of whether microbial reactions can contribute significantly to bicarbonate generation relative to mineral reactions remains open. In carbonate aquifers, reaction between carbonic acid and carbonate minerals is likely the dominant source of bicarbonate production. However, in silicic aquifers, we hypothesize that the bicarbonate contribution of microbial reactions can be dominant, depending on the rate at which electron donors are supplied. Where the flux of electron donors into the system is relatively high, microbial reactions have the potential to generate bicarbonate more rapidly than mineral reactions. Simulations designed to predict the fate of CO₂ within such systems may underestimate the rate of carbon trapping if they do not account for microbial reactions (Kirk et al., 2013).

3.6. Implications for water quality

In contrast to the benefit of enhanced CO₂ trapping, an increase in the relative significance of iron reduction has the potential to negatively affect water quality by leading to higher dissolved iron concentrations and affecting the stability of oxide and sulfide minerals. Both solid-phases provide important sinks for many hazardous solutes in aqueous environments. Arsenic, for example, can strongly sorb to iron oxides and oxyhydroxides or be sequestered by sulfide minerals such as pyrite (Smedley and Kinniburgh, 2002). If CO₂ leakage shifts the balance between iron reduction and sulfate reduction, as predicted by our analysis, then the rate at which sulfide minerals form and remove arsenic from water would decrease while the rate at which oxides dissolve and release arsenic increases. Shifts in microbial activity predicted by our analysis, therefore, favor enhance mobility of hazardous solutes such as arsenic.

3.7. Concluding comments

We carried out biogeochemical modeling to analyze how CO₂ leakage impacts the

thermodynamics and kinetics of microbial reactions in two different aquifers – a carbonate-free aquifer of limited pH buffering capacity and a calcite-rich aquifer that effectively buffers pH change. The simulation results showed that CO₂ leakage influences the thermodynamics of microbial reactions, including reduction potentials of different redox couples and the energy available to microbial functional groups. For the common electron donors and acceptors in aquifers (table 1), their reduction potentials increase with the increase in CO₂ partial pressure. The increases are different for different electron donors and acceptors, and are larger in the carbonate-free aquifer than in the calcite-rich aquifer.

The available energy of different functional groups responds differently to the leakage of CO₂. With the increase in CO₂ partial pressure, the energy available to syntrophs and to acetoclastic methanogen decreases, while the energy available to iron reducers and hydrogenotrophic sulfate reducer and methanogen increases. Considering the control of the available energy on microbial rates, these results suggest that CO₂ leakage may inhibit the metabolisms of syntrophs and acetoclastic methanogen, but promote the metabolisms of iron reducers and hydrogenotrophic sulfate reducer and methanogen.

We tested these predictions by carrying out two kinetic simulations of microbial metabolisms in the hypothetical calcite-rich aquifer. The first simulation focused on the response of H₂-, acetate-, and lactate-oxidizing sulfate reducers, and the second explored the competition between sulfate reducers and iron reducers. The results showed that CO₂ leakage favors microbial iron reduction and inhibits microbial sulfate reduction, which are consistent with the predictions from the thermodynamics. The results also show that, in the absence of iron reducers, CO₂ leakage has little impact on hydrogenotrophic sulfate reduction, a prediction that differs from the thermodynamic prediction.

These modeling exercises illustrate the complexity in microbiological response to CO₂ leakage. Our analysis is limited in that it only considered the overall reactions of microbial respiration, without accounting for biochemical mechanism or microbial physiology. Nevertheless, the results suggest that the impact of CO₂ leakage on aquifer microorganisms is complex – different microbial reactions respond differently to CO₂ leakage: some metabolisms are favored, others are depressed, and still others remain unchanged. Because high CO₂ abundance impacts the physiology of microorganisms, it is tempting to speculate that actual microbiological responses would be more complex than what we have demonstrated here.

These modeling exercises also illustrate the power of coupled thermodynamic and kinetic analysis of microbial reactions. Thermodynamic and kinetic analyses are routine tasks in today's biogeochemical studies. The thermodynamic analysis is on the basis of chemical thermodynamic properties, and tells whether or not, under given geochemical conditions, a microbial reaction is favored by thermodynamics. The kinetic modeling combines thermodynamic properties of chemical substances with kinetic parameters of microbial metabolisms, and predicts how fast microbes catalyze chemical reactions and reproduce themselves.

So far the thermodynamic and kinetic analyses have often been carried out separately. This study combined the two analyses to predict the microbiological impact of CO₂ leakage. The results of both methods support the conclusion that different microbial reactions respond

840 differently to the leakage of CO₂. Importantly, the kinetic analysis places a quantitative
841 constraint on the thermodynamic predictions. For example, the thermodynamic analysis
842 suggested that CO₂ leakage promotes hydrogenotrophic sulfate reduction, but depresses sulfate
843 reduction by lactate oxidation. The kinetic analysis showed that CO₂ leakage does not change
844 significantly the rates of the two reactions. For lactate-oxidizing sulfate reduction, this is because
845 the change in the available energy is relatively small; for hydrogenotrophic sulfate reduction, the
846 rate increase by increasing available energy is balanced by the rate decrease by decreasing H₂
847 availability in the environment. These predictions represent example hypotheses generated by the
848 thermodynamic and kinetic analysis that can be further tested using laboratory and field
849 experiments.

References

- Apps, J.A., Zheng, L., Zhang, Y., Xu, T., and Birkholzer, J.T. (2010). Evaluation of potential changes in groundwater quality in response to CO₂ leakage from deep geologic storage. *Transport in Porous Media* 82, 215-246.
- Benson, S.M., and Cole, D.R. (2008). CO₂ sequestration in deep sedimentary formations. *Elements* 4, 325-331.
- Bertoloni, G., Bertucco, A., De Cian, V., and Parton, T. (2006). A study on the inactivation of micro-organisms and enzymes by high pressure CO₂. *Biotechnology and Bioengineering* 95, 155-160.
- Bethke, C.M. (2008). *Geochemical and Biogeochemical Reaction Modeling*. Cambridge, UK: Cambridge University Press.
- Bethke, C.M., Sanford, R.A., Kirk, M.F., Jin, Q., and Flynn, T.M. (2011). The thermodynamic ladder in geomicrobiology. *American Journal of Science* 311, 183-210.
- Bigham, J.M., Schwertmann, U., Traina, S.J., Winland, R.L., and Wolf, M. (1996). Schwertmannite and the chemical modeling of iron in acid sulfate waters. *Geochimica et Cosmochimica Acta* 60, 2111-2121.
- Celia, M.A., and Nordbotten, J.M. (2009). Practical modeling approaches for geological storage of carbon dioxide. *Ground Water* 47, 627-638.
- Chapelle, F.H. (2001). *Ground-Water Microbiology and Geochemistry*. New York: John Wiley & Sons, Inc.
- Dean, A.P., Lynch, S., Rowland, P., Toft, B.D., Pittman, J.K., and White, K.N. (2013). Natural wetlands are efficient at providing long-term metal remediation of freshwater systems polluted by acid mine drainage. *Environmental Science & Technology* 47, 12029-12036.
- Delany, J.M., and Lundeen, S.R. (1990). "The LLNL thermodynamical database". Lawrence Livermore National Laboratory Report UCRL-21658).
- Dixit, S., and Hering, J.G. (2006). Sorption of Fe(II) and As(III) on goethite in single- and dual-sorbate systems. *Chemical Geology* 228, 6-15.
- Emerson, J.B., Thomas, B.C., Alvarez, W., and Banfield, J.F. (2015). Metagenomic analysis of a high carbon dioxide subsurface microbial community populated by chemolithoautotrophs and bacteria and archaea from candidate phyla. *Environmental Microbiology*.
- Flynn, T.M., Sanford, R.A., Ryu, H., Bethke, C.M., Levine, A.D., Ashbolt, N.J., and Santo Domingo, J.W. (2013). Functional microbial diversity explains groundwater chemistry in a pristine aquifer. *BMC Microbiology* 13.
- Gerlach, R., and Cunningham, A.B. (2010). "Influence of Biofilms on Porous Media Hydrodynamics," in *Porous Media: Applications in Biological Systems and Biotechnology*, ed. K. Vafai. (New York: CFC Press), 173-230.
- Gislason, S.R., Wolff-Boenisch, D., Stefansson, A., Oelkers, E.H., Gunnlaugsson, E., Sigurdardottir, H., Sigfusson, B., Broecker, W.S., Matter, J.M., Stute, M., Axelsson, G., and Fridriksson, T. (2010). Mineral sequestration of carbon dioxide in basalt: A pre-injection overview of the CarbFix project. *International Journal of Greenhouse Gas Control* 4, 537-545.
- Gunter, W.D., Wiwchar, B., and Perkins, E.H. (1997). Aquifer disposal of CO₂-rich greenhouse gases: Extension of the time scale of experiment for CO₂-sequestering reactions by geochemical modelling. *Mineralogy and Petrology* 59, 121-140.

- Harvey, O.R., Qafoku, N.P., Cantrell, K.J., Lee, G., Amonette, J.E., and Brown, C.F. (2013). Geochemical implications of gas leakage associated with geological CO₂ storage - a qualitative review. *Environmental Science & Technology* 47, 23-36.
- Helgeson, H.C. (1969). Thermodynamics of hydrothermal systems at elevated temperatures and pressures. *American Journal of Science* 267, 729-804.
- Humez, P., Negrel, P., Lagneau, V., Lions, J., Kloppmann, W., Gal, F., Millot, R., Guerrot, C., Flehoc, C., Widory, D., and Girard, J.F. (2014). CO₂-water-mineral reactions during CO₂ leakage: Geochemical and isotopic monitoring of a CO₂ injection field test. *Chemical Geology* 368, 11-30.
- Inagaki, F., Kuypers, M.M.M., Tsunogai, U., Ishibashi, J., Nakamura, K., Treude, T., Ohkubo, S., Nakaseama, M., Gena, K., Chiba, H., Hirayama, H., Nunoura, T., Takai, K., Jorgensen, B.B., Horikoshi, K., and Boetius, A. (2006). Microbial community in a sediment-hosted CO₂ lake of the southern Okinawa Trough hydrothermal system. *Proceedings of the National Academy of Sciences of the United States of America* 103, 14164-14169.
- Ingraham, J.L. (1987). "Effect of temperature, pH, water activity, and pressure on growth," in *Escherichia coli and Salmonella typhimurium: Cellular and Molecular Biology*, eds. F.C. Neidhardt, J.L. Ingraham, K.B. Low, B. Magasanik, M. Schaechter & H.E. Umbarger. (Washington, D.C.: American Society for Microbiology), 1543-1554.
- Ippc (2005). "Special Report on Carbon Capture and Storage". Available at <http://www.ipcc.ch/>.
- Jin, Q. (2012). Energy conservation of anaerobic respiration. *American Journal of Science* 312, 573-628.
- Jin, Q., and Bethke, C.M. (2003). A new rate law describing microbial respiration. *Applied and Environmental Microbiology* 69, 2340-2348.
- Jin, Q., and Bethke, C.M. (2005). Predicting the rate of microbial respiration in geochemical environments. *Geochimica et Cosmochimica Acta* 69, 1133-1143.
- Jin, Q., and Bethke, C.M. (2007). The thermodynamics and kinetics of microbial metabolism. *American Journal of Science* 307, 643-677.
- Jin, Q., and Roden, E.E. (2011). Microbial physiology-based model of ethanol metabolism in subsurface sediments. *Journal of Contaminant Hydrology* 125, 1-12.
- Jin, Q., Roden, E.E., and Giska, J.R. (2013). Geomicrobial kinetics: extrapolating laboratory studies to natural environments. *Geomicrobiology Journal* 30, 173-185.
- Kampman, N., Bickle, M., Becker, J., Assayag, N., and Chapman, H. (2009). Feldspar dissolution kinetics and Gibbs free energy dependence in a CO₂-enriched groundwater system, Green River, Utah. *Earth and Planetary Science Letters* 284, 473-488.
- Keating, E., Newell, D., Dempsey, D., and Pawar, R. (2014). Insights into interconnections between the shallow and deep systems from a natural CO₂ reservoir near Springerville, Arizona. *International Journal of Greenhouse Gas Control* 25, 162-172.
- Keating, E.H., Newell, D.L., Viswanathan, H., Carey, J.W., Zyvoloski, G., and Pawar, R. (2013). CO₂/Brine Transport into Shallow Aquifers along Fault Zones. *Environmental Science & Technology* 47, 290-297.
- Kharaka, Y.K., Cole, D.R., Hovorka, S.D., Gunter, W.D., Knauss, K.G., and Freifeld, B.M. (2006). Gas-water-rock interactions in Frio Formation following CO₂ injection: Implications for the storage of greenhouse gases in sedimentary basins. *Geology* 34, 577-580.

- Kharaka, Y.K., Thordsen, J.J., Hovorka, S.D., Nance, H.S., Cole, D.R., Phelps, T.J., and Knauss, K.G. (2009). Potential environmental issues of CO₂ storage in deep saline aquifers: Geochemical results from the Frio-I Brine Pilot test, Texas, USA. *Applied Geochemistry* 24, 1106-1112.
- Kharaka, Y.K., Thordsen, J.J., Kakouros, E., Ambats, G., Herkelrath, W.N., Beers, S.R., Birkholzer, J.T., Apps, J.A., Spycher, N.F., Zheng, L.E., Trautz, R.C., Rauch, H.W., and Gullickson, K.S. (2010). Changes in the chemistry of shallow groundwater related to the 2008 injection of CO₂ at the ZERT field site, Bozeman, Montana. *Environmental Earth Sciences* 60, 273-284.
- Kirk, M.F., Altman, S.J., Santillan, E.F.U., and Bennett, P.C. (2016). Interplay between microorganisms and geochemistry in geological carbon storage. *International Journal of Greenhouse Gas Control* 47, 386-395.
- Kirk, M.F., Jin, Q., and Haller, B.R. (2015). Broad-scale evidence that pH influences the balance between microbial iron and sulfate reduction. *Groundwater*, n/a-n/a.
- Kirk, M.F., Santillan, E.F.U., Sanford, R.A., and Altman, S.J. (2013). CO₂-induced shift in microbial activity affects carbon trapping and water quality in anoxic bioreactors. *Geochimica et Cosmochimica Acta* 122, 198-208.
- Langmuir, D. (1997). *Aqueous Environmental Geochemistry*. Upper Saddle River, New Jersey: Prentice-Hall, Inc.
- Lide, D.R. (2003). *Handbook of Chemistry and Physics* Boca Raton, Florida: CRC Press.
- Lindsay, M.B.J., Moncur, M.C., Bain, J.G., Jambor, J.L., Ptacek, C.J., and Blowes, D.W. (2015). Geochemical and mineralogical aspects of sulfide mine tailings. *Applied Geochemistry* 57, 157-177.
- Lions, J., Devau, N., De Lary, L., Dupraz, S., Parmentier, M., Gombert, P., and Dictor, M.C. (2014). Potential impacts of leakage from CO₂ geological storage on geochemical processes controlling fresh groundwater quality: A review. *International Journal of Greenhouse Gas Control* 22, 165-175.
- Little, M.G., and Jackson, R.B. (2010). Potential impacts of leakage from deep CO₂ geosequestration on overlying freshwater aquifers. *Environmental Science & Technology* 44, 9225-9232.
- Liu, C., Kota, S., Zachara, J.M., Fredrickson, J.K., and Brinkman, C.K. (2001). Kinetic analysis of the bacterial reduction of goethite. *Environmental Science and Technology* 35, 2482-2490.
- Lovley, D.R., and Chapelle, F.H. (1995). Deep subsurface microbial processes. *Reviews of Geophysics* 33, 365-382.
- Lu, J.M., Partin, J.W., Hovorka, S.D., and Wong, C. (2010). Potential risks to freshwater resources as a result of leakage from CO₂ geological storage: a batch-reaction experiment. *Environmental Earth Sciences* 60, 335-348.
- Matter, J.M., and Kelemen, P.B. (2009). Permanent storage of carbon dioxide in geological reservoirs by mineral carbonation. *Nature Geoscience* 2, 837-841.
- Mitchell, A.C., Phillips, A.J., Hamilton, M.A., Gerlach, R., Hollis, W.K., Kaszuba, J.P., and Cunningham, A.B. (2008). Resilience of planktonic and biofilm cultures to supercritical CO₂. *Journal of Supercritical Fluids* 47, 318-325.
- Noguera, D.R., Brusseau, G.A., Rittmann, B.E., and Stahl, D.A. (1998). A unified model describing the role of hydrogen in the growth of *Desulfovibrio vulgaris* under different environmental conditions. *Biotechnology and Bioengineering* 59, 732 - 746.

- Oppermann, B.I., Michaelis, W., Blumenberg, M., Frerichs, J., Schulz, H.M., Schippers, A.,
Beaubien, S.E., and Kruger, M. (2010). Soil microbial community changes as a result of
long-term exposure to a natural CO₂ vent. *Geochimica et Cosmochimica Acta* 74, 2697-
2716.
- Oule, M.K., Tano, K., Bernier, A.M., and Arul, J. (2006). *Escherichia coli* inactivation
mechanism by pressurized CO₂. *Canadian Journal of Microbiology* 52, 1208-1217.
- Park, J., Sanford, R.A., and Bethke, C.M. (2006). Geochemical and microbiological zonation of
the Middendorf aquifer, South Carolina. *Chemical Geology* 230, 88-104.
- Peet, K.C., Freedman, A.J.E., Hernandez, H.H., Britto, V., Boreham, C., Ajo-Franklin, J.B., and
Thompson, J.R. (2015). Microbial Growth under Supercritical CO₂. *Applied and
Environmental Microbiology* 81, 2881-2892.
- Price, P.B., and Sowers, T. (2004). Temperature dependence of metabolic rates for microbial
growth, maintenance, and survival. *Proceedings of the National Academy of Sciences*
101, 4631-4636.
- Roden, E.E. (2006). Geochemical and microbiological controls on dissimilatory iron reduction.
Comptes Rendus Geosciences 338, 456-467.
- Roden, E.E. (2008). "Microbiological controls on geochemical kinetics 1: Fundamentals and
case study on microbial Fe(III) oxide reduction," in *Kinetics of Water-Rock Interaction*,
eds. S.L. Brantley, J.D. Kubicki & A.F. White. (New York: Springer), 335-415.
- Roden, E.E., and Urrutia, M.M. (2002). Influence of biogenic Fe(II) on bacterial crystalline
Fe(III) oxide reduction. *Geomicrobiology Journal* 19, 209-251.
- Santillan, E.U., Kirk, M.F., Altman, S.J., and Bennett, P.C. (2013). Mineral influence on
microbial survival during carbon sequestration. *Geomicrobiology Journal* 30, 578-592.
- Shao, H.B., Qafoku, N.P., Lawter, A.R., Bowden, M.E., and Brown, C.F. (2015). Coupled
geochemical impacts of leaking CO₂ and contaminants from subsurface storage reservoirs
on groundwater quality. *Environmental Science & Technology* 49, 8202-8209.
- Sherlock, E.J., Lawrence, R.W., and Poulin, R. (1995). On the neutralization of acid rock
drainage by carbonate and silicate minerals. *Environmental Geology* 25, 43-54.
- Smedley, P.L., and Kinniburgh, D.G. (2002). A review of the source, behaviour, and distribution
of arsenic in natural waters. *Applied Geochemistry* 17, 517-568.
- Stumm, W., and Morgan, J.J. (1996). *Aquatic Chemistry. Chemical Equilibria and Rates in
Natural Waters*. New York: John Wiley & Sons, Inc.
- Tuttle, J.H., Dugan, P.R., and Randles, C.I. (1969). Microbial sulfate reduction and its potential
utility as an acid mine water pollution abatement procedure. *Applied Microbiology* 17,
297- 302.
- Videmsek, U., Hagn, A., Suhadolc, M., Radl, V., Knicker, H., Schlöter, M., and Vodnik, D.
(2009). Abundance and diversity of CO₂-fixing bacteria in grassland soils close to natural
carbon dioxide springs. *Microbial Ecology* 58, 1-9.
- Wang, S., and Jaffe, P.R. (2004). Dissolution of a mineral phase in potable aquifers due to CO₂
releases from deep formations; effect of dissolution kinetics. *Energy Conversion and
Management* 45, 2833-2848.
- Wilkin, R.T., and Digiulio, D.C. (2010). Geochemical impacts to groundwater from geologic
carbon sequestration: Controls on pH and inorganic carbon concentrations from reaction
path and kinetic modeling. *Environmental Science & Technology* 44, 4821-4827.
- Wimmer, Z., and Zarevucka, M. (2010). A review on the effects of supercritical carbon dioxide
on enzyme activity. *International Journal of Molecular Sciences* 11, 233-253.

- 1031 Wu, B., Shao, H.B., Wang, Z.P., Hu, Y.D., Tang, Y.J.J., and Jun, Y.S. (2010). Viability and
1032 metal reduction of *Shewanella oneidensis* MR-1 under CO₂ stress: Implications for
1033 ecological effects of CO₂ leakage from geologic CO₂ sequestration. *Environmental*
1034 *Science & Technology* 44, 9213-9218.
- 1035 Xu, T.F., Apps, J.A., and Pruess, K. (2005). Mineral sequestration of carbon dioxide in a
1036 sandstone-shale system. *Chemical Geology* 217, 295-318.
- 1037 Yakimov, M.M., Giuliano, L., Crisafi, E., Chernikova, T.N., Timmis, K.N., and Golyshin, P.N.
1038 (2002). Microbial community of a saline mud volcano at San Biagio-Belpasso, Mt. Etna
1039 (Italy). *Environmental Microbiology* 4, 249-256.
- 1040 Zhang, J., Davis, T.A., Matthews, M.A., Drews, M.J., Laberge, M., and An, Y.H. (2006).
1041 Sterilization using high-pressure carbon dioxide. *Journal of Supercritical Fluids* 38, 354-
1042 372.
- 1043 Zheng, L.G., Apps, J.A., Zhang, Y.Q., Xu, T.F., and Birkholzer, J.T. (2009). On mobilization of
1044 lead and arsenic in groundwater in response to CO₂ leakage from deep geological storage.
1045 *Chemical Geology* 268, 281-297.
1046

1047 Table 1. Reduction reactions of common electron donors and acceptors in aquifers, and their
1048 standard reduction potentials $E^{\circ'}$ at pH 7^(a).

Half-reaction	$E^{\circ'}$ (mV)
$8\text{H}^+ + 8\text{e}^- \rightarrow 4\text{H}_2(\text{aq})$	-506.2
$2\text{Acetate} + 2\text{HCO}_3^- + 10\text{H}^+ + 8\text{e}^- \rightarrow 2\text{Lactate} + 4\text{H}_2\text{O}$	-438.0
$2\text{Acetate} + 10\text{H}^+ + 8\text{e}^- \rightarrow 2\text{Ethanol} + 2\text{H}_2\text{O}$	-390.3
$8\text{Goethite} + 24\text{H}^+ + 8\text{e}^- \rightarrow 8\text{Fe}^{2+} + 16\text{H}_2\text{O}$	-389.7
$\frac{4}{3}\text{HCO}_3^- + \frac{28}{3}\text{H}^+ + 8\text{e}^- \rightarrow \frac{4}{3}\text{Methanol} + \frac{8}{3}\text{H}_2\text{O}$	-373.7
$4\text{Acetate} + 10\text{H}^+ + 8\text{e}^- \rightarrow 2\text{Butyrate} + 4\text{H}_2\text{O}$	-284.8
$2\text{HCO}_3^- + 9\text{H}^+ + 8\text{e}^- \rightarrow \text{Acetate} + 4\text{H}_2\text{O}$	-279.1
$\frac{4}{3}\text{Acetate} + \frac{4}{3}\text{HCO}_3^- + \frac{28}{3}\text{H}^+ + 8\text{e}^- \rightarrow \frac{4}{3}\text{Propionate} + 4\text{H}_2\text{O}$	-278.7
$\text{HCO}_3^- + 9\text{H}^+ + 8\text{e}^- \rightarrow \text{CH}_4(\text{aq}) + 3\text{H}_2\text{O}$	-259.6
$\text{SO}_4^{2-} + 9\text{H}^+ + 8\text{e}^- \rightarrow \text{HS}^- + 4\text{H}_2\text{O}$	-217.0

1049
1050 (a) Standard reduction potential at 1 atm, 25 °C, and pH 7 is calculated from the updated LLNL
1051 Thermodynamic Database (Delany and Lundeen, 1990).

1052 Table 2. Redox reactions, standard available energy at pH 7.

Redox reaction	$\Delta G_A^{\circ'}$ (kJ·mol ⁻¹)
Syntrophic oxidation	
1. Acetate+4H ₂ O ⇌ CH ₃ CO ₂ ⁻ + 2HCO ₃ ⁻ + H ⁺	-175.25
2. 2Lactate+4H ₂ O ⇌ 2CH ₃ CO ₂ ⁻ + 4H ₂ (aq)+2HCO ₃ ⁻ + 2H ⁺	-52.65
3. $\frac{4}{3}$ Propionate+4H ₂ O ⇌ $\frac{4}{3}$ CH ₃ CO ₂ ⁻ + 4H ₂ (aq)+ $\frac{4}{3}$ HCO ₃ ⁻ + $\frac{4}{3}$ H ⁺	-175.58
4. 2Butyrate+4H ₂ O ⇌ 2CH ₃ CO ₂ ⁻ + 4H ₂ (aq)+2H ⁺	-170.90
5. $\frac{4}{3}$ Methanol+ $\frac{8}{3}$ H ₂ O ⇌ $\frac{4}{3}$ CH ₃ CO ₂ ⁻ + $\frac{4}{3}$ HCO ₃ ⁻ + $\frac{4}{3}$ H ⁺	-102.24
6. 2Ethanol+2H ₂ O ⇌ 2CH ₃ CO ₂ ⁻ + 4H ₂ (aq)+2H ⁺	-89.42
Goethite reduction	
7. 4H ₂ (aq)+8Goethite+16H ⁺ ⇌ 4CH ₃ CO ₂ ⁻ + 8Fe ²⁺	89.90
8. Acetate+8Goethite+15H ⁺ ⇌ CH ₃ CO ₂ ⁻ + 12H ₂ O + 8Fe ²⁺	-85.35
9. 2Lactate+8Goethite+14H ⁺ ⇌ 2CH ₃ CO ₂ ⁻ + 12H ₂ O + 8Fe ²⁺	37.25
10. $\frac{4}{3}$ Propionate+8Goethite+12 $\frac{2}{3}$ H ⁺ ⇌ $\frac{4}{3}$ CH ₃ CO ₂ ⁻ + $\frac{4}{3}$ HCO ₃ ⁻ + 12H ₂ O + 8Fe ²⁺	-85.68
11. 2Butyrate+8Goethite+14H ⁺ ⇌ 2CH ₃ CO ₂ ⁻ + 12H ₂ O + 8Fe ²⁺	-81.00
12. $\frac{4}{3}$ Methanol+8Goethite+ $\frac{44}{3}$ H ⁺ ⇌ $\frac{4}{3}$ CH ₃ CO ₂ ⁻ + 8Fe ²⁺ + $\frac{40}{3}$ H ₂ O	-12.34
13. 2Ethanol+8Goethite+14H ⁺ ⇌ 2CH ₃ CO ₂ ⁻ + 8Fe ²⁺ + 14H ₂ O	0.48
Sulfate reduction	
14. 4H ₂ (aq)+SO ₄ ²⁻ +2H ⁺ ⇌ 4H ₂ O + H ₂ S	223.23
15. Acetate+SO ₄ ²⁻ +H ⁺ ⇌ CH ₃ CO ₂ ⁻ + H ₂ S	47.97

16.	$2\text{Lactate} + \text{SO}_4^{2-} \rightarrow \text{Acetate} + 2\text{HCO}_3^- + \text{H}_2\text{S}$	170.57
17.	$\frac{4}{3}\text{Propionate} + \text{SO}_4^{2-} + \frac{2}{3}\text{H}^+ \rightarrow \frac{4}{3}\text{Acetate} + \frac{4}{3}\text{HCO}_3^- + \text{H}_2\text{S}$	47.64
18.	$2\text{Butyrate} + \text{SO}_4^{2-} \rightarrow \text{Acetate} + \text{H}_2\text{S}$	52.33
19.	$\frac{4}{3}\text{Methanol} + \text{SO}_4^{2-} + \frac{2}{3}\text{H}^+ \rightarrow \frac{4}{3}\text{H}_2\text{O} + \frac{4}{3}\text{HCO}_3^-$	120.98
20.	$2\text{Ethanol} + \text{SO}_4^{2-} \rightarrow \text{Acetate} + \text{H}_2\text{S} + 2\text{H}_2\text{O}$	133.80
Methanogenesis		
21.	$4\text{H}_2(\text{aq}) + \text{H}^+ + \text{HCO}_3^- \rightarrow \text{Acetate}(\text{aq}) + 3\text{H}_2\text{O}$	190.33
22.	$\text{Acetate} + \text{H}_2\text{O} \rightarrow \text{CO}_2 + \text{CH}_4(\text{aq})$	15.07

1053

1054 Table 3. Redox reactions, kinetic parameters (rate constant k , and half-saturation constant K_D and K_A), growth parameters (growth yield Y and
1055 specific maintenance rate D), and thermodynamic parameters (ATP yield m_P and average stoichiometric number χ) of microbial functional
1056 groups.

Functional group	Redox reaction ^(a)	Kinetic parameter ^(b)			Growth parameter		Thermodynamic parameter ^(c)	
		k (mol·g ⁻¹ ·s ⁻¹)	K_D (molal)	K_A (molal)	$Y^{(c)}$ (g·mol ⁻¹)	$D^{(d)}$ (s ⁻¹)	m_P	χ
Syntroph ^(e)	2	1.0×10^{-5}	5.0×10^{-2}	— ^(f)	13.8	10^{-8}	2.76	4
Iron reducers	7	$1.5 \times 10^{-5(g)}$	1.0×10^{-6}	$7.0^{(h)}$	7.8	10^{-8}	2.0	8
	8	$1.5 \times 10^{-5(g)}$	1.2×10^{-5}	$7.0^{(h)}$	5.6	10^{-8}	1.5	8
	9	$1.5 \times 10^{-5(g)}$	$5.2 \times 10^{-4(i)}$	$7.0^{(h)}$	14.7	10^{-8}	3.0	8
Sulfate reducers	14	1.0×10^{-6}	1.1×10^{-6}	3.9×10^{-5}	5.0	10^{-8}	1.0	6
	15	1.0×10^{-6}	5.0×10^{-6}	3.9×10^{-5}	4.6	10^{-8}	0.75	6
	16	1.0×10^{-6}	2.0×10^{-4}	3.9×10^{-5}	14.6	10^{-8}	2.25	6
Methanogens	21	1.0×10^{-6}	4.7×10^{-6}	— ^(f)	1.25	10^{-8}	0.25	2
	22	1.0×10^{-6}	2.3×10^{-5}	— ^(f)	2.5	10^{-8}	0.5	2

- 1057
1058 (a) See table 2.
1059 (b) Jin and Roden (2011)
1060 (c) Jin (2012)
1061 (d) Price and Sowers (2004)
1062 (e) Parameters are estimated based on the experimental observations of Noguera et al. (1998, their fig 3).
1063 (f) No electron acceptor dependence.
1064 (g) Unit is s⁻¹.
1065 (h) Unit is g cell dry weight per mol of bioavailable surface sites, i.e., g·mol⁻¹.
1066 (i) Liu et al. (2001)

Figure legends

Figure 1. Conceptual model for biogeochemical reaction modeling. Na-Cl water containing sulfate flows through a quartzite aquifer confined between aquitards. In the aquitards, natural organic matter is degraded to H₂, acetate, lactate, and other electron donors (D), which diffuse into the aquifer. CO₂ from a deep storage reservoir migrates upwards along a fault into the aquifer. The aquifer is seeded with small initial populations of microbial functional groups that can grow on lactate, acetate, and H₂ by using goethite, sulfate, bicarbonate, and proton as electron acceptors.

Figure 2. Variations in pH and concentrations of calcium (Ca²⁺), dissolved CO₂(aq), bicarbonate, and calcium-bicarbonate complex (CaHCO₃⁺) with CO₂ partial pressure in a hypothetical carbonate-free (A and B) and calcite-rich aquifer (C and D).

Figure 3. Variations in relative abundances of monohydrogen sulfide (HS⁻), acetate, lactate, propionate, butyrate, and their conjugate acids with CO₂ partial pressure in a hypothetical carbonate-free (A) and calcite-rich aquifer (B).

Figure 4. Variations in the ionic strength of groundwater (A) and the activity coefficients of ions (B) with CO₂ partial pressure in a hypothetical calcite-rich aquifer.

Figure 5. Variations in reduction potentials E of redox couples with CO₂ partial pressure in a hypothetical carbonate-free (A) and calcite-rich aquifer (B). Labels show the redox couples; see table 1 for reduction reactions.

Figure 6. Variations in the available energy ΔG_A to syntrophic oxidation, goethite reduction, sulfate reduction, and methanogenesis in a hypothetical carbonate-free (A to D) and calcite-rich (E to H) aquifer. Labels show the electron donors of redox reactions; see table 2 for reaction equations.

Figure 7. Functional groups supported by the electron donors of H₂, acetate, and lactate, and the resulting reaction network (also see table 2). FeRM, ferric iron reducer; SRM, sulfate reducer; MG, methanogen; Syn, syntroph.

Figure 8. Variations with time in CO₂ partial pressure (A) and pH (B) in a hypothetical calcite-rich aquifer.

Figure 9. Variations with time in the concentrations of H₂, acetate, lactate (A), and sulfide (B), the biomass concentrations of sulfate reducers (C), the rates of sulfate reduction (D), the energy available to sulfate reducers (E), the thermodynamic factor F_T (F), the kinetic factor of sulfate (F_A), H₂, and acetate (F_D), and specific growth rate of acetotrophic sulfate reducer in the hypothetical calcite-rich aquifer.

Figure 10. Variations with time in the concentrations of H₂, acetate, lactate (A), sulfide, ferrous iron (B), the bioavailable surface sites >FeOH, and sorbed ferrous iron >FeOFe⁺ (C), the biomass concentrations of iron reducers and sulfate reducers (D), the rates of iron reduction and sulfate reduction (E), the energy available to iron reducers (F), and the thermodynamic factor F_T of iron reducers (G) in the hypothetical calcite-rich aquifer.

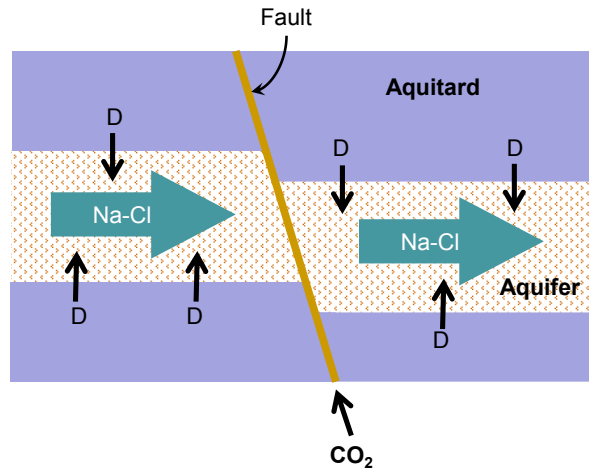


Fig. 1

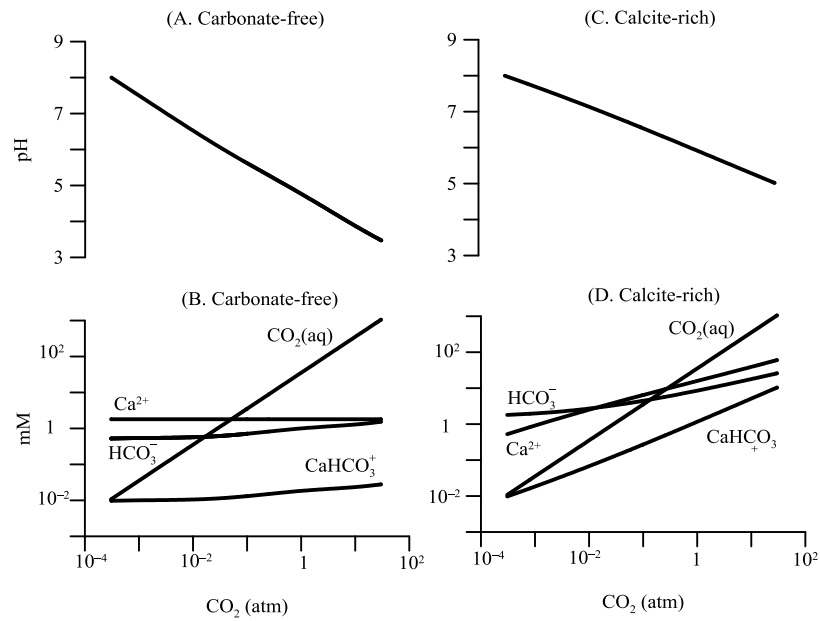


Fig. 2

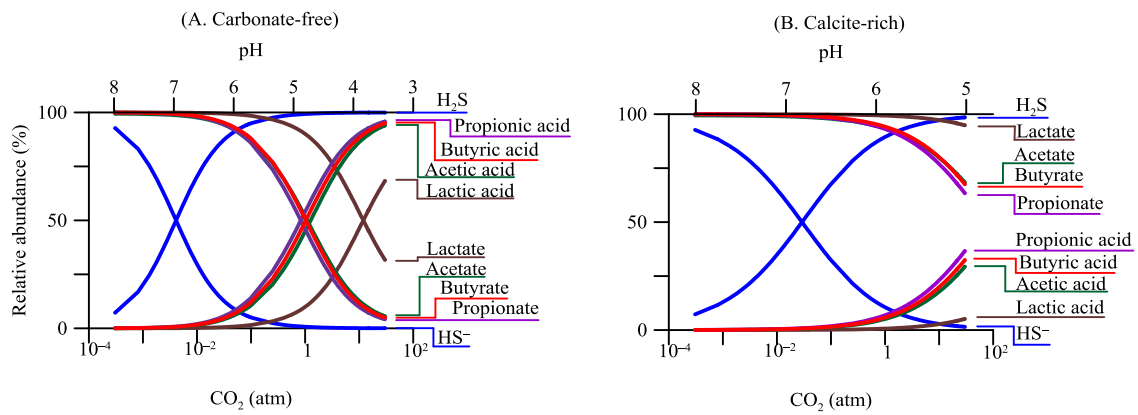


Fig. 3

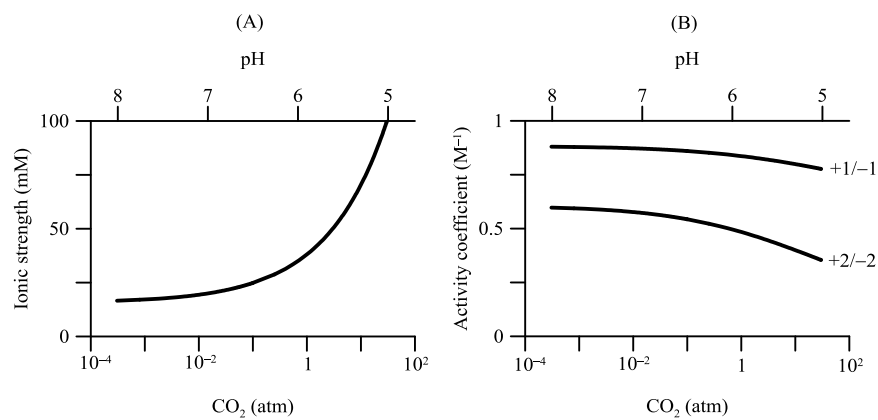


Fig. 4

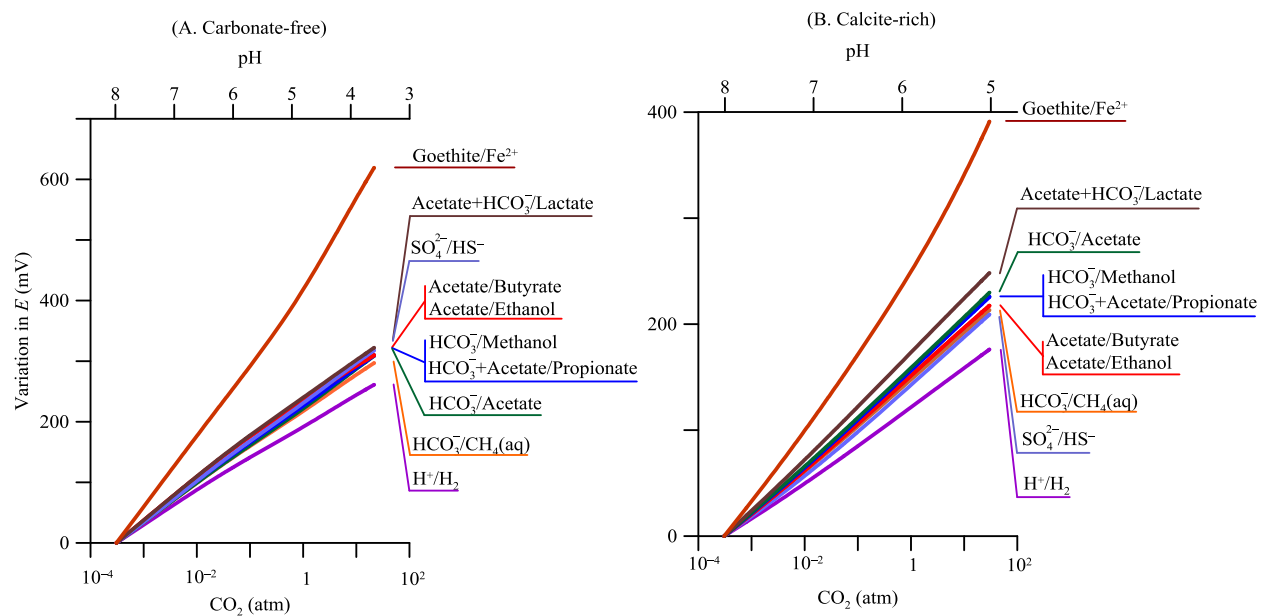


Fig. 5

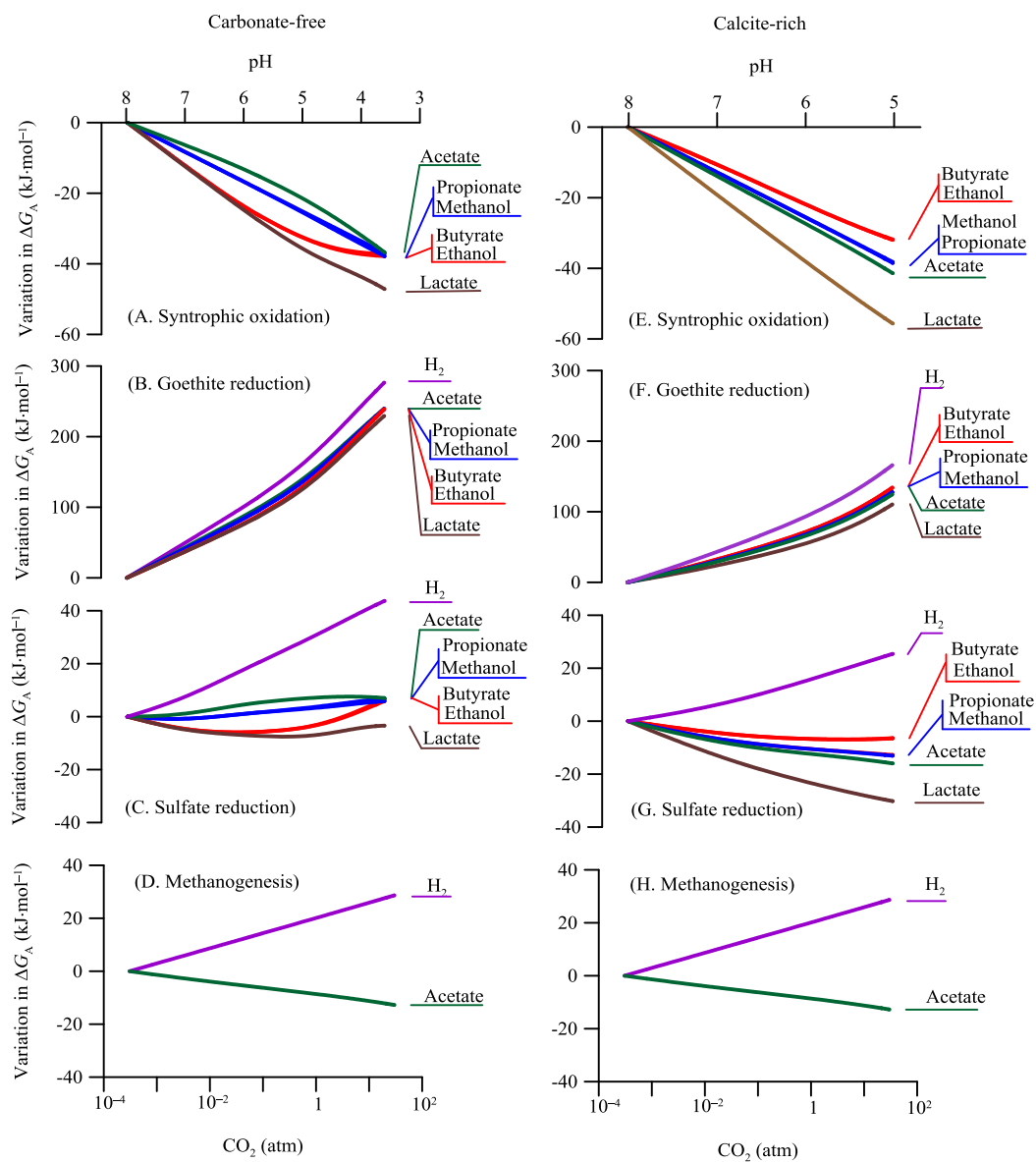


Fig. 6

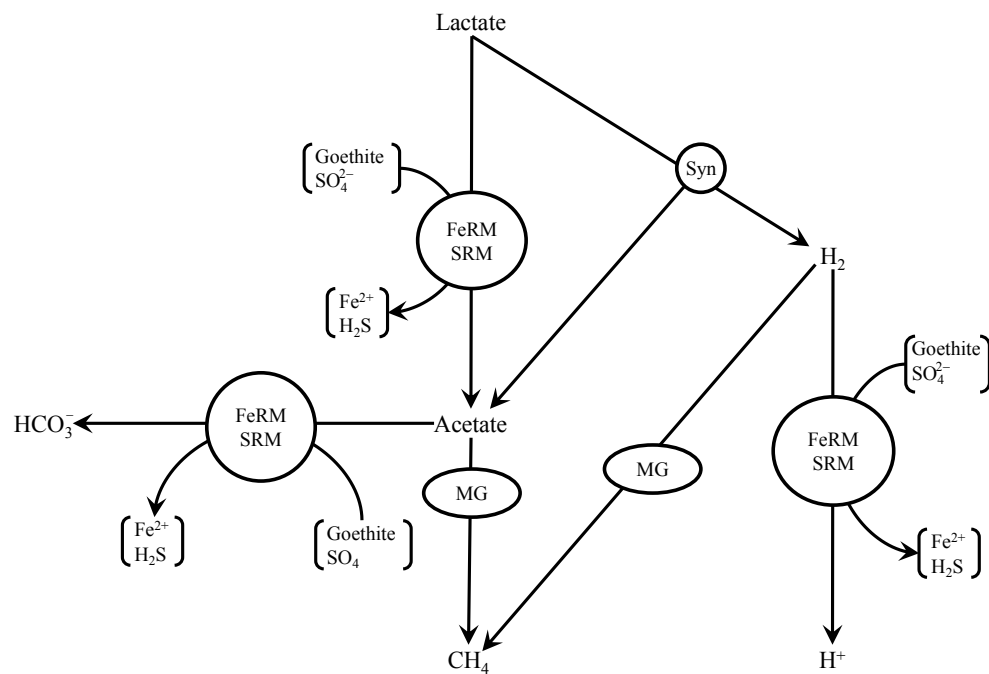


Fig. 7

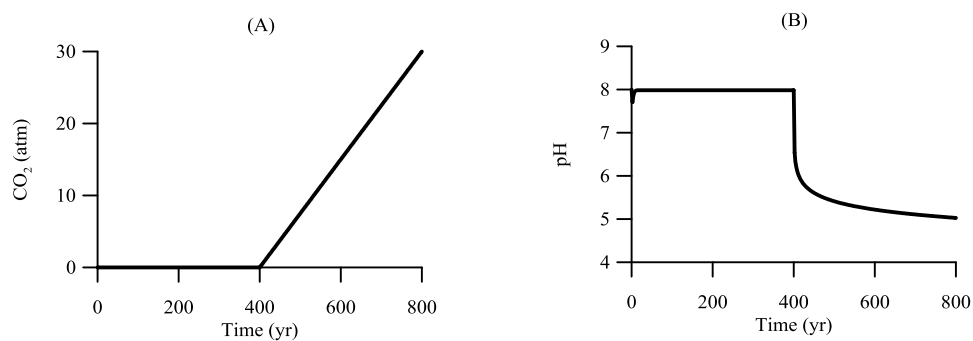


Fig. 8

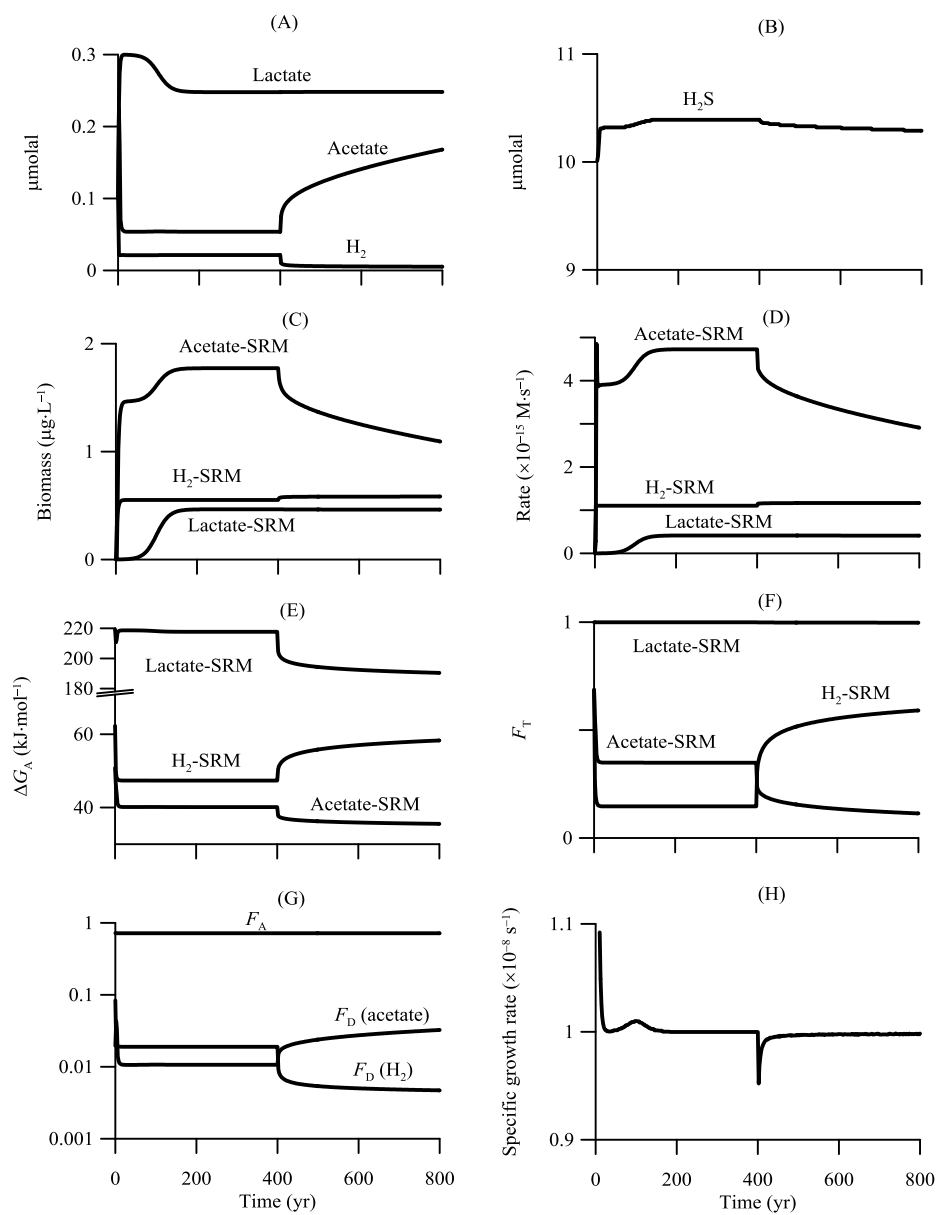


Fig. 9

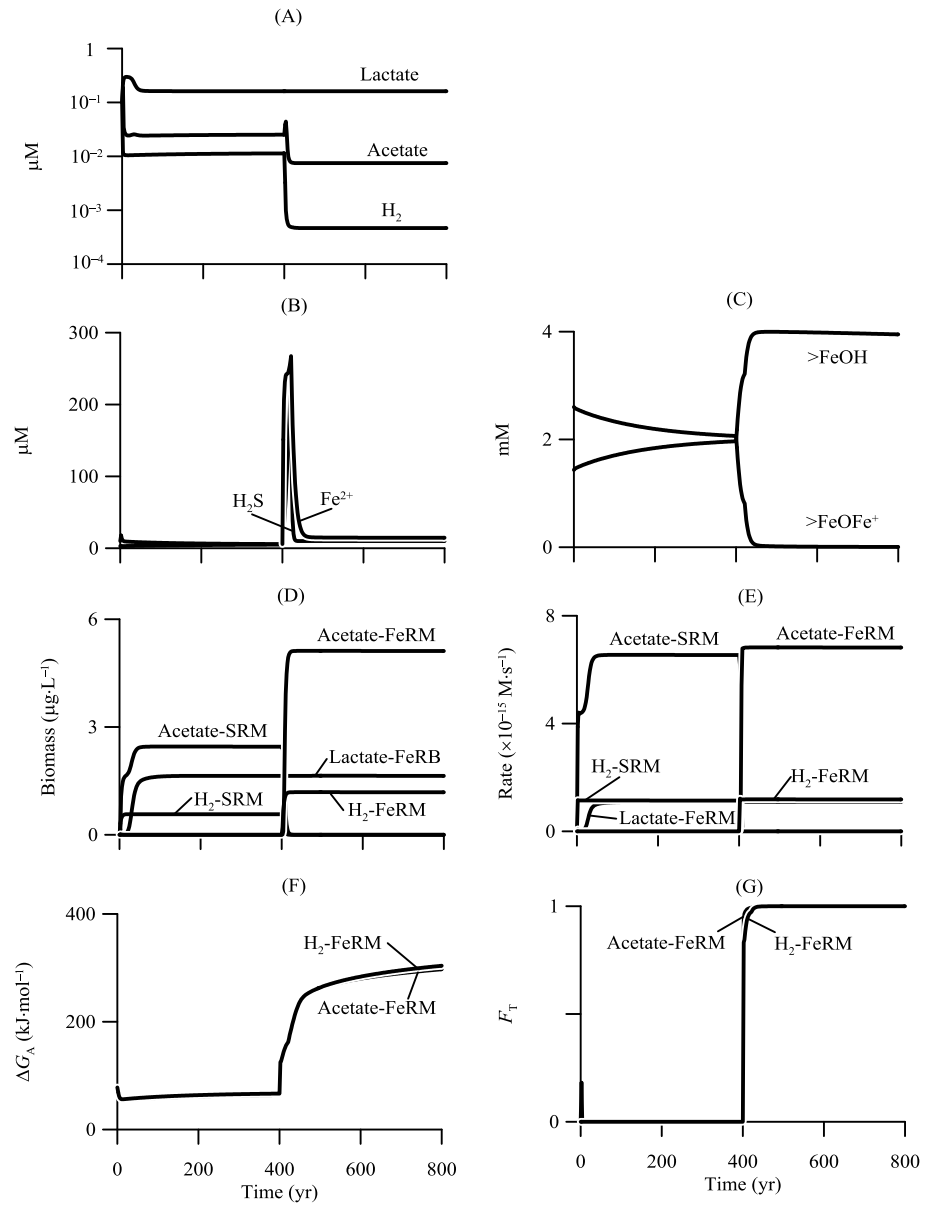


Fig. 10